The Origin of Adhesive Nanoscopic Friction

by

Zazo Meijs

A thesis submitted in partial fulfillment for the
degree of Master of Physics and Astronomy

in the
Faculty of Science, Amsterdam

Daily Supervisor: Dr. Bart Weber
Supervisor: Prof. Steve Franklin
Second examiner: Prof. Joost Frenken
Content: 60 EC

September 2019

Atoms on a small scale behave like nothing on a large scale, for they satisfy the laws of quantum mechanics.

- Richard Feynman [1]

[1] From Feynman's famous lecture: Plenty of Room at the Bottom [1]

UNIVERSITY OF AMSTERDAM

Abstract

Faculty of Science, Amsterdam

Master of Sciene, Physics and Astronomy

by Zazo Meijs

The invention of the Atomic Force Microscope in 1982 [2] has allowed us to probe topography in the nanometer scale. At this scale, otherwise considered flat surfaces are rough and the observed macroscopic friction becomes a sum of many single asperity interactions. However, even 37 years after its invention we do not understand the mechanism by which friction dissipates energy in these non-destructive single asperity interactions. Within this project we have investigated the use of *Lateral Force Microscopy* (LFM) to measure friction forces on a single asperity. We have succeeded in calibrating both the normal and lateral stiffness of our system. We Furthermore, investigated the method's ability to measure adhesion forces and estimate the radius of the tip apex through deconvolution. Evaluation of the tip also allows us to measure the wear of a single asperity system. We present a novel theory which describes friction as an energy dissipation through delocalized phonons. As phonons are periodic excitations of the crystalline structure, their numbers are limited in nano-scale structures which contain a limited number of atoms. To test the theory, we produced islands through *Focused Ion Beam* (FIB) milling and performed local friction measurements through LFM. We have not found a friction dependence on the size of our nano-patterns. However, we have found a correlation between the friction and the effective stiffness of the tip and surface interface. Furthermore, we were able to use the developed LFM method to measure single asperity friction in different environments, opening a new path of nanoscale friction and wear research.

Acknowledgements

Foremost, I would like to express my deep gratitude to doctor Bart Weber, for giving me the opportunity to work on this project and for his excellent supervision of this thesis work. I am likewise greatly indebted to Feng-Chun Hsia for his help with both the experimental work and the interpretation.

I would like to thank both my Examiners; Professor Steve Franklin, Contact Dynamics group leader, who was invaluable when it came to thinking about the industrial and applications of this work, specifically to the ASML case, and Professor Joost Frenken whose continued creativity and enthusiasm formed the basis of many parts of this thesis, most notably regarding the main theory of adhesive friction. On this note, I would also like to thank Professor Sergey Krylov from the Russian Academy of Sciences in Moscow, who on two different occasions came to Amsterdam in part to discuss the results of this project and whose theoretical insights are central to our conclusions.

I would also like to thank the rest of the Contact Dynamics group; Sander de Graaf, Cyrian Leriche, Doctor Fiona Elam and most importantly Daan Haver, who was with me for the whole duration and who was always my first source of advice if I was stuck. All of them have given valuable input and asked critical questions to deepen my understanding of the subject.

For both intellectual and otherwise awesome conversations I have to thank the whole of ARCNL, who were all extremely welcoming and approachable to me as a master student. Particularly the NanoLayers group; Görsel Yetik, Victor Vollema, Cristina Sfiligoj and Kuan-Da Huang, whose lunchtime conversations taught much about their projects, my own project and science in general. I would like to thank the Personnel Club ('Personeels vereniging') for both the delightful events they held and for allowing me to join the Personnel Club, making me truly feel like part of the institute.

Furthermore, I am grateful for the support by the technical staff, both here at ARCNL and at the AMOLF nanolab. Specifically, I'd like to thank Arend-Jan van Calcar, who was always available for technical assistance and advise at ARCNL and Andries Lof who, taught me too (and immensely helped we with) operating the FIB and SEM at AMOLF.

Last but not least, I want to thank my friends, family, roommates and my lovely girlfriend for their continued support even when (the writing of) this thesis took up all my time.

Contents

Chapter 1

Introduction

Friction is among the most fundamental phenomena studied in physics. Everywhere surfaces move over surfaces, friction occurs, slowing this movement and causing energy loss. This loss is significant, and impacts both environment and industry; it is estimated that frictional energy dissipation is responsible for up to 23% of the global energy use [3]. However, the origin of frictional dissipation remains unclear.

Examples of our pursuit to control friction were already recorded in ancient Egypt. Tomb drawings from 2400 BC depict the pouring of water on sand in front of large sleds that transport heavy stones [4]. The first written scientific work on friction is credited to Leonardo da Vinci [5], and was followed upon by Amontons, who in 1699 formulated Amontons' first law. Amonton showed that the friction force increases linearly with the applied normal force in all dry systems [6]. Although this description is over 300 years old, it is still the most widely used friction law for macroscopic systems. However, to date we do not understand the mechanism by which friction causes energy dissipation during sliding.

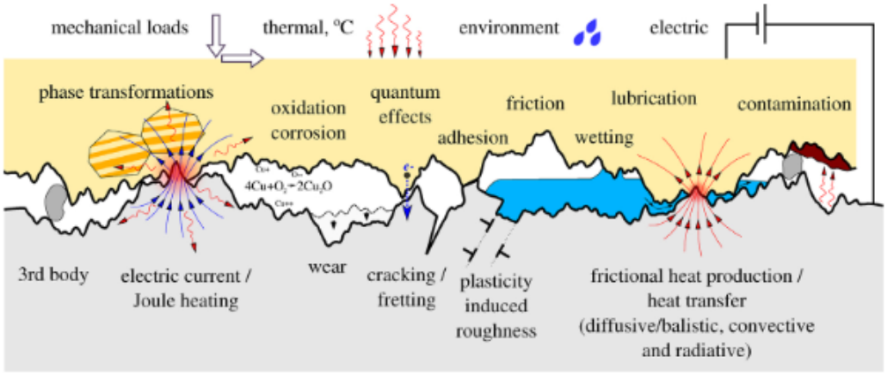

FIGURE 1.1: A schematic representing the many different effects that influence friction and wear [7]

From experiments we know that macroscopic friction is a combination of many effects, various of which are environmental, as illustrated in figure 1.1. The first thing to realize is that macroscopic surfaces are not atomically smooth. Figure 1.2 illustrates how, as we zoom in on a flat on flat surface, we see that there actually is an interaction between asperities. This means that the observed, macroscopic friction originates at a multitude of these single-asperity contacts. It is by studying the behaviour of such single-asperity contacts (under controlled conditions) that we aim to contribute to a fundamental theory of friction and wear.

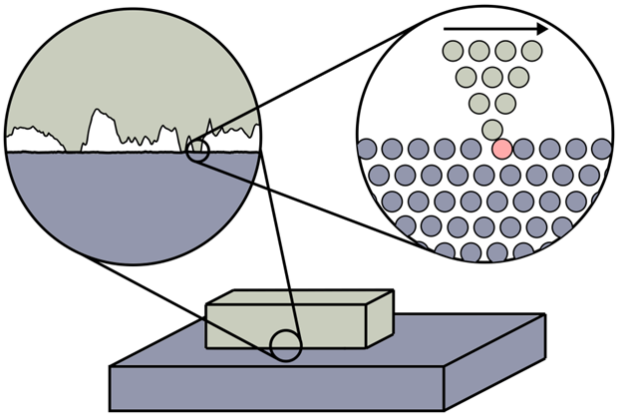

FIGURE 1.2: Zoom in to nanoscale

This project was also motivated by the desire to understand a specific example of friction, which occurs commonly during the nano-lithography phase of the fabrication of silicon electronics. This research thesis was completed at the *Advanced Research Center for Nano-Lithography* (ARCNL) within the Contact Dynamics group lead by Professor Steve Franklin. As such, the project is part of a broader effort aimed at understanding and manipulating the friction and wear behaviour at the 'silicon-wafer'-on-'wafer-table' interfaces that play an important role in the performance of Nano-Lithography machines. From simple experiments, we know that the friction that occurs during the nano-lithography stage is most likely adhesive friction. Figure 1.3 shows the surface topography (height) of the wear scar on a sapphire sphere that was worn as a result of sliding motion on a Silicon wafer using a Bruker *Universal Mechanical Tester* (UMT) in a test that resembles the sliding behavior that occurs in nano-lithography machines.[1] The horizontal profile shows that the wear scar is smooth down to the nanometer level, showing no wear on scales larger than molecules. We observe no transfer of material and the ball has to be displace significantly (∼1000 atomic spacings) to remove a single atomic layer. This all supports the hypothesis that we are dealing with adhesive friction. This is exactly the type of friction we will be studying in our experiments.

[1] It should be noted that this figure has artifacts, the top and bottom are not higher, resulting in a completely flat wear scar

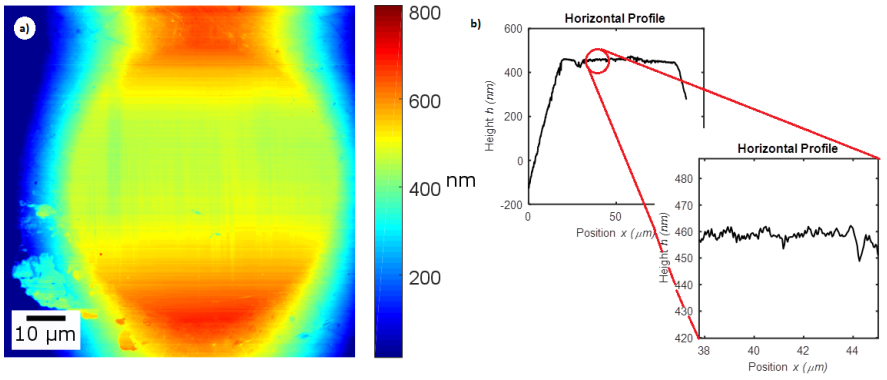

FIGURE 1.3: PeakForce tapping-mode scan of the wear track on a Sapphire sphere.

To investigate the behavior of single-asperity contacts, we use an *Atomic Force Microscope* (AFM) which brings nanometer sharp tips into contact with flat substrates and can measure normal and tangential forces at the interface. This technique is referred to as *Lateral Force Microscopy* (LFM) and is detailed in chapter 2. The main question investigated within this thesis is the origin of adhesive friction at atomic scales. Recently, a phonon-based model of the mechanism by which sliding motion is damped was developed by Frenken and Krylov [8]. Within this model, the localized displacement at a strained single-asperity contact is described as the sum of many phonons, which are de-localized vibrations in the system. When the contact slips, the strain is released and the resulting motion of the asperity is strongly damped because the phonons run out of phase with one another. This phononic description of frictional damping is treated in detail in chapter 3. Furthermore, chapter 3 discusses how frictional damping can be manipulated through nano-structuring the sliding surfaces; an effect that may have been observed recently [9]. In chapter 4 LFM experiments performed on nano-structured surfaces are presented. In chapter 5 we will discuss the implications of these results and the relevant effects that need to be taken into account. In chapter 6 we will concisely report the conclusions of this project and how it is embedded in future work of the group.

Finally, side questions investigated during this project are discussed in the appendices. Appendix A discusses tip evaluation through Scanning Electron Microscopy (SEM). Appendix B discusses observed humidity dependence in the pull-off force and observed speed dependence for the friction. Appendix C introduces Peakforce tapping mode, a Bruker patented AFM mode which is optimal for the tip radius calibration and gives extra interesting local information, including local adhesive forces. Appendix D discusses single-asperity friction under Vapour Phase Lubrication (VPL) with isopropanol to compliment other macroscale research within the group. Lastly, appendix E presents a poster on local friction measurements, which was presented at the *Utrecht Scanning Probe Microscopy Day 2018*.

Chapter 2

LFM local friction measurements

To measure the friction experienced by a single asperity we use an *Atomic Force Microscope* (AFM). We use a commercial AFM from Bruker[1]. In *Lateral Force Microscopy* (LFM), an atomically sharp tip is forced to slide over a substrate while the normal and lateral force are measured. This lateral force is then related to friction interaction between tip and sample. Using this setup we can measure contacts of a few *nanometers*. Much work was done on characterizing our setup and calibrating the *Voltage outputs* to *Newton* observables.

In this chapter we will first discuss how an AFM works in general. In the following (sub)sections we discuss how we use LFM. Starting with the ramping procedure to calibrate the sensitivity (section 2.3), which also gives us the adhesion force on our tip. We will explain the *Thermal Tune* used to calibrate the stiffness of our sample (section 2.3.1). With the deflection sensitivity and stiffness we can calibrate the applied normal force (section 2.4) and the torsion stiffness (section 2.5 of the cantilever to transform our voltage outputs into force measurements. We discuss the used tips in section 2.6 and how to measure the tip apex through deconvolution in section 2.7. The last section (2.8) discusses the use of Fourier Transforms to find periodic behaviour and test for external noise.

In the appendices we discuss further details of the AFM/LFM process; In appendix B we discuss the effect of Humidity on Adhesion and the speed dependence of nanoscale friction. In appendix C we present the PeakForce-Tapping mode which is an extension to the widely used Scan-Assist mode, but also gives local adhesion measurements.

[1] Dimension Icon with ScanAsyst capabilities

2.1 Working of Atomic Force Microscopy

To understand the working of the Lateral Force Microscopy it is essential to first discus the Atomic Force Microscope (AMF) in a more general sense. First introduced in IBM labs by *Binnig et al* in 1986 [2], the AFM has become a standard method to measure the topography of samples with *nanometer* precision [10]. A schematic representation of an AFM is shown in figure 2.1a. The AFM consists of a cantilever, at the end of which a sharp tip touches the surface. The tip is moved with respect to the sample by a piezo element which is connected to the other side of the cantilever. Forces exerted at the tip-on-surface interface result in deformation of the cantilever which is measured by deflected laser light.

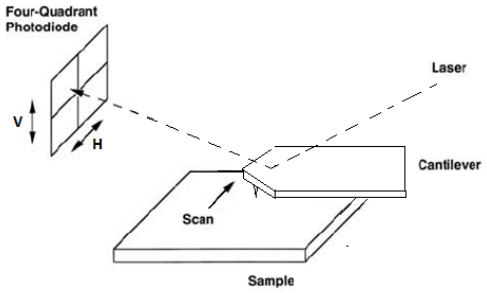

(A) Schematic of the AFM

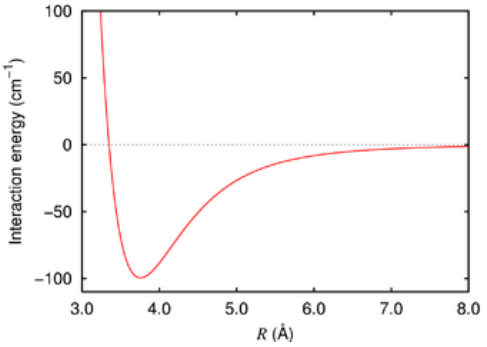

(B) The Lennard-Jones potential describing the interaction between tip and sample as function of their separation.

The height of the cantilever is controlled by a closed loop photo-diode system. The measured deflection is kept constant by changing the voltage on the piezo which controls the height of the cantilever. The interaction between the tip and the surface can be approximated by the *Lennard-Jones potential* (figure 2.1b). Important to notice is that as we bring two objects within a few Angstrom they repel each other, until at 0 separation they repel each other infinitely (Pauli exclusion principle). As we separate them we reach a point where instead of repelling each other they start attracting each other through the *Van der Waals force*. This behaviour is described by the Lennard-Jones Potential, given by;

$$V(r) = \frac{A}{r^{12}} - \frac{B}{r^6} \tag{2.1}$$

where A and B are positive real values.

2.2 Lateral Force Microscopy

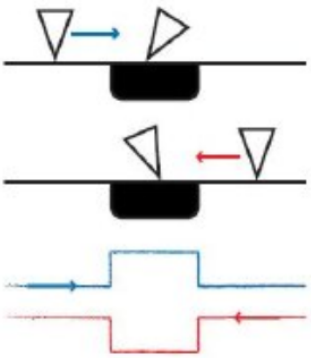

(A) Schematic of how an increase in COF of the sample influences the force loop.

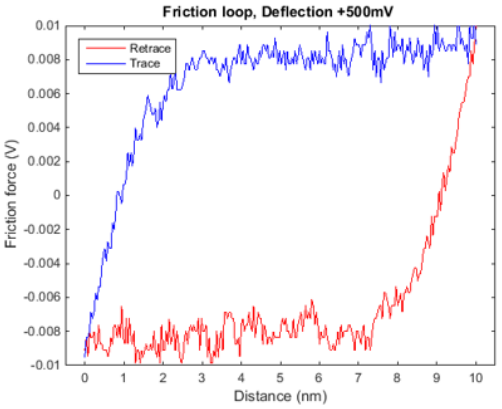

(B) Example Force Loop as the AFM takes for each scanned line.

Lateral Force Microscopy (LFM) is a contact mode of AFM for which we look at both the normal deflection and the torsional deflection of the cantilever. The normal deflection gives us the height profile, as in general *contact AFM*, while the lateral deflection is dependent on the friction. When we plot a single line of the lateral torsion we get a force loop, figure 2.2b, which is created by the Trace (forward stroke) and Retrace (return stroke). The lateral deflection is the horizontal photo-diode and is in Volts, to transform this to a force we need to calibrate the lateral is stiffness which is non-trivial and explained in section 2.5. If we can calculate the force which was applied to rotate the cantilever, we get a force over distance. By taking the area under the curve we get an energy (*Force*Distance* = *Energy*) which is the energy dissipated by friction. It is important for later chapters to keep in mind that within this method the Friction force is measured through a loss of energy. To compare our nano-scale results with macro-scale ones it is desirable to have a classical Friction force for which we can simply take

$$F_{fric} = \frac{Trace(Fric) - Retrace(Fric)}{2}$$

.

But this gives us a friction force in *Volts* and from classical tribology we know that this friction force should depend on the applied normal force which we can also only set in Volts [2].

[2]Within the newest version of NanoScope one can choose a normal force in nN, if the Deflection Sensitivity (DS) and cantilever Stiffnes (k) are calibrated.

2.3 Adhesion force / ramping

To calibrate the cantilever deformation per *Volt* supplied to the z-piezo (called the *Deflection Sensitivity* (DS) [nm/V]), we perform a 'ramp'. The ramping procedure is shown in figure 2.3. First, the tip approaches the sample till a contact interaction is measured. After contact it is returned a specified distance back up to be in equilibrium position (point 1). The tip approaches the surface with a set approach speed (always 100 nm/s for all our measurements, important to keep constant as it does strongly influence the measured adhesion [11]) till 'snap-in' (point 2). After 'snap-in', the tip is pushed down till the measured deflection reaches the *force limit* (point 3). We now know that our *force limit* is the equilibrium voltage plus the absolute value of the trigger threshold which we set in the ramping parameters. As we reach the *force limit*, we withdraw the cantilever with equal velocity till 'Snap-off' (point 4 to 5). It is important to note that 'snap-off' is much larger than 'snap-in', implying that there is an increase in adhesion force when the till stays on the surface. The vertical distance between 'snap-off' and 'Out of contact' (point 5 to 6) is because of the adhesion force that keeps the tip in contact without external force. As the external pulling force overcomes the adhesion force, the tip detaches and returns to equilibrium position (point 7).

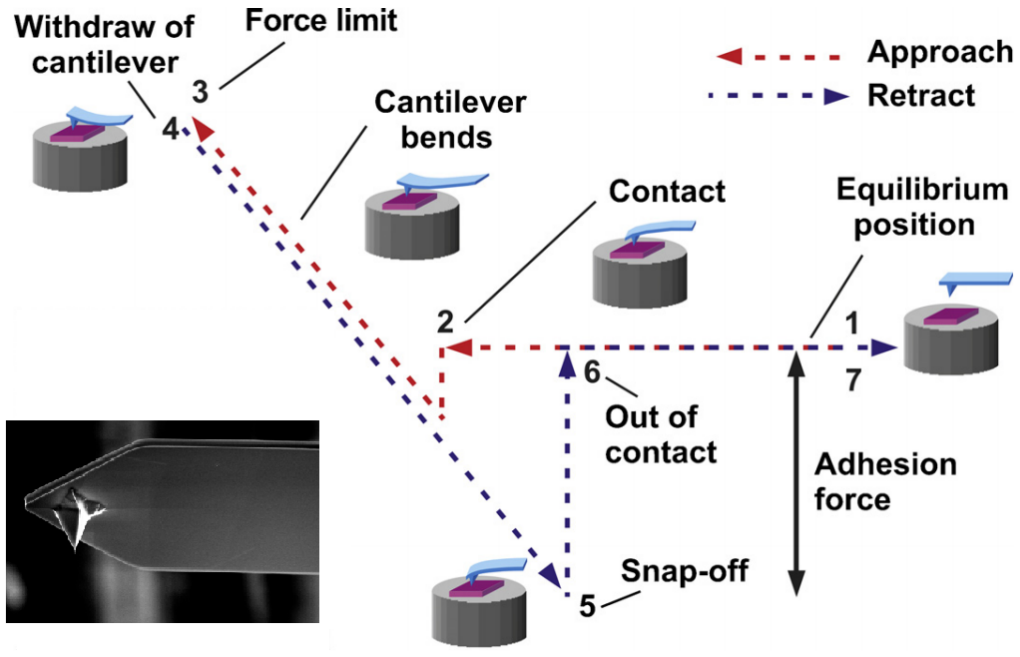

FIGURE 2.3: Schematic presentation of what happens during the ramping procedure. Image copied from [12], inset is an Electron Microscopy image of an ESPA-V2 tip.

At first, we tried to use negative trigger thresholds (which is comparable to the force limit in figure 2.3) to mimic negative deflection setpoints so we would have the real Adhesion force for each measurement. The data in figure 2.4 clearly shows that negative trig

threshold values have the same effect as their positive counterparts. This corresponds to figure 2.3 where the Force limit it always above the equilibrium value. The effect of a negative trig threshold would be unclear. The question of why an increase in trigger threshold increases the adhesion force is discussed in literature and is two-old. Firstly, as we increase the trigger threshold, we also increase the time during which the tip is in contact, which has been shown to increase adhesion force [13]. Secondly, the higher trig threshold corresponds to a higher normal force which increases the effective contact area [14] which might result in a higher adhesive force. This confirms that even though the *Deflection Setpoint*, which controls the normal force when scanning, is an absolute value, the *ramping threshold* is relative around zero. Furthermore, we have done first measurements of the Adhesion dependence on Relative Humidity, for which the details can be found in appendix B. [miss die appendix gewoon hier toevoegen? ik weet niet wat beter is?]

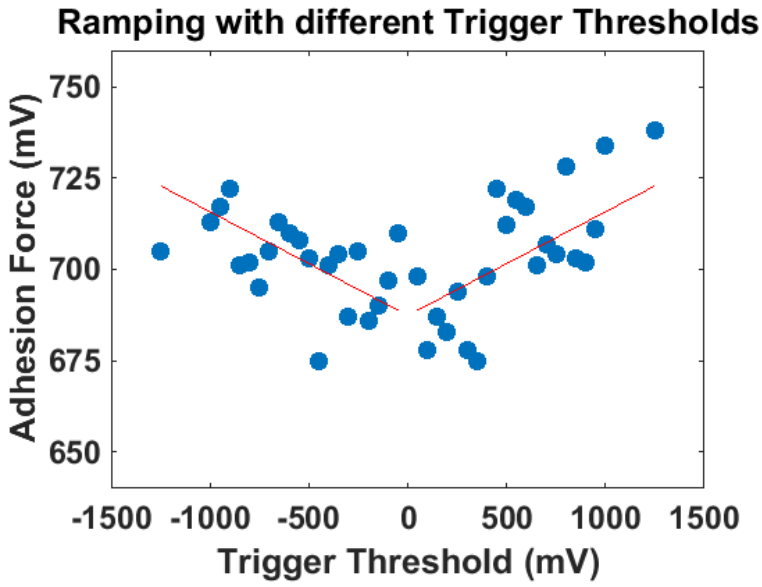

FIGURE 2.4: Adhesion force dependence on trigger threshold, the fit is made using all the data, and mirrored around zero.

2.3.1 Thermal Tune

After calibrating the Deflection Sensitivity (section 2.3) we calibrate the normal stiffness by the Bruker method; *thermal tune*. The normal stiffness (k) is the amount of force needed to displace the cantilever in the normal direction (N/m). Thermal tune is done by suspending the cantilever away from contact, at which point the vibrations by thermal excitation are measured. The amount of energy supplied to the system is in the order of $k_B * T$; where k_B is Boltzmann constant and T is the temperature in Kelvin. The induced movement is measured and a Power Spectral Density (PSD) is taken (see figure

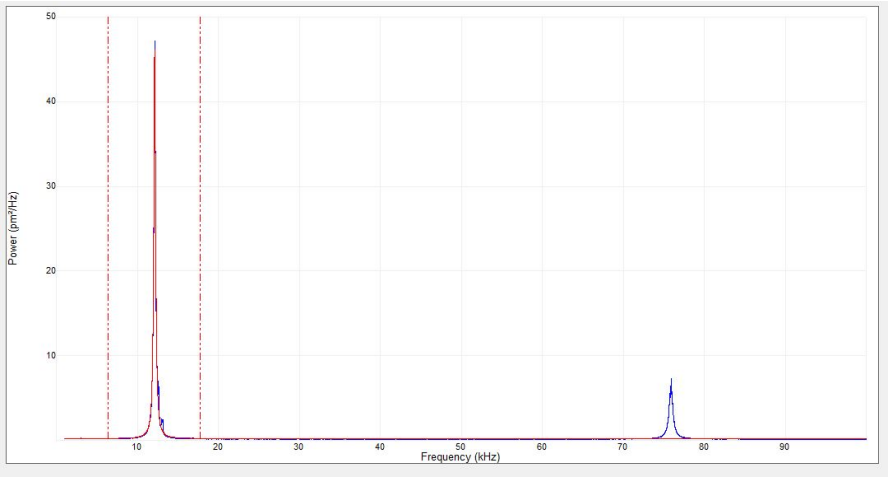

FIGURE 2.5: An example thermal tune PSD for a ESPA-V2 tip

2.5). In the PSD we see a large peak, which corresponds to the eigenvalue peak. By integrating over this peak (minus the noise), we get the amount of energy in our system (P). We can now calculate the stiffness k by,

$$k = \frac{k_B * T}{P} \tag{2.2}$$

The Bruker *Thermal Tune* process [3] is based on the the work by Hutter et al. in 1993 [15]. This method is considered very suitable for soft cantilevers ($k < 1N/m$) but is only an approximation at much stiffer cantilevers[16]. The relevance of this method is confirmed in the recent work on mechanical resonance of nano-wires by Hsia et al. in 2019[17].

It is important to note that the resulting stiffness is also based on the supplied Deflection Sensitivity (DS). As the deflection by thermal excitation is measured again through the photo-diode, it is taken into account when calculating the power (P) in the *eigenpeak* [is that a real term?]. Therefore it is important to first calibrate the deflection sensitivity before calibrating the stiffness. As the deflection sensitivity was measured while constrained on two sides, and it is only constrained on one side for thermal tune, we need to take a correction factor into account. Literature shows that we underestimate the amplitude by approximately 8% [18], which translates to a Deflection Sensitivity correction of 1.08 in the fit parameters. The fit also depends linearly on Temperature as we can see from equation 2.2. The temperate in the lab only fluctuates a few degrees at most around room-temperature so we do not expect this error to be significant to our data.

[3] `http://www.nanophys.kth.se/nanophys/facilities/nfl/afm/fast-scan/bruker-help/Content/Probe%20and%20Sample%20Guide/ThermalTune/ThermalTune.htm`

2.4 Normal Force Calibration

The Normal Force (F_N) is the force perpendicular to the sample with which it pushes against the tip to keep it from indenting the surface. As it is a reaction force it is equal in magnitude to the force with which the tip pushes against the surface. In macroscopic systems, the normal force is often a result of gravitation. In our experiments, it is always a mechanically applied and controlled force.

The photo-diode measures the normal force indirectly through the deflection of the cantilever, in Volts. To translate the deflection measurement it is necessary to calibrate the measurement. In figure 2.6 we see the photo-diode as shown by the AFM. The most important factor is the vertical Photo-Diode-Offset (V_{offset}), which is advised by the manual to put at -2 Volt. If you then apply a reasonable normal force, around 2V or 100nN for our soft tips, the measured deflection would be around zero, giving you optimal sensitivity [ref]. It is always advised to keep the 'Horizontal Deflection' as close as possible to 0 V.

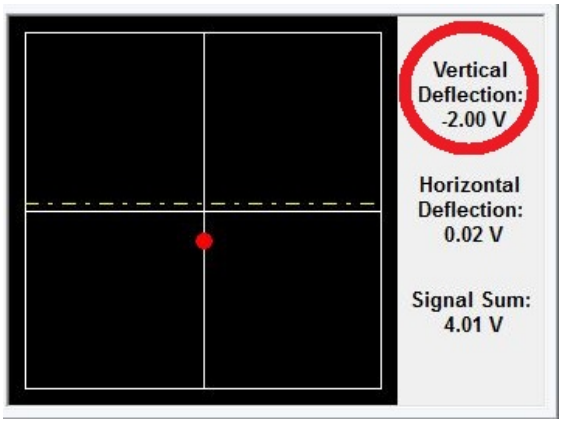

FIGURE 2.6: The photo-diode output as shown by the AFM software. The vertical deflection (red circle) will be referred to as the Photo-Diode-Offset (V_{offset}) throughout this thesis. The horizontal deflection should always be 0V, while the SUM signal is set at 4 Volts (both with ± 0.02 V error)

The scan parameter that controls the normal force is the Deflection-Setpoint (V_{Defl}). The applied normal deflection (in *Volts*) depends on the Deflection-Setpoint and Photo-diode-offset according to;

$$F_N(V) = V_{Defl} - V_{offset} \tag{2.3}$$

We have done three sets of friction measurements at different photo-diode-offsets and varying Deflection setpoints. The results are presented in figure 2.7. As we shift the

normal force with the photo-diode-offsets, we see clear overlap in the measured frictions which confirms the validity of this interpretation.

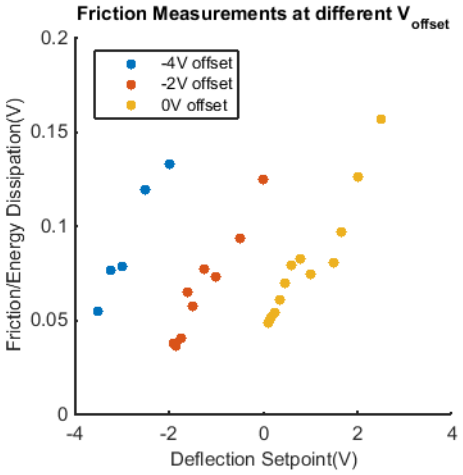

(A) Friction measurements for different offset values and varying the Deflection setpoint

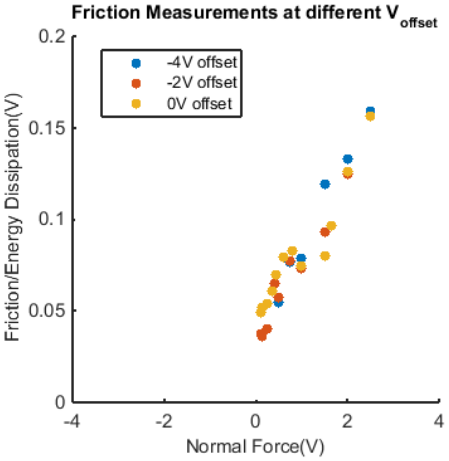

(B) Friction measurements shifted for different offset values to get $F_n(V)$

FIGURE 2.7

To calculate the normal force in *Newtons*, we need the Deflection Sensitivity (DS) and the normal stiffness (k). The deflection sensitivity describes the relation between the cantilever deflection (nm) and the photo-diode signal (V). The deflection sensitivity can be calibrated through the ramping procedure, explained in section 2.3. The normal stiffness (k) is the stiffness of the cantilever in the direction perpendicular to the sample. Each cantilever is supplied with an approximate stiffness and we can calibrate a more precise stiffness by thermal tune, as explained in section 2.3.1. By multiplying the total normal deflection with the deflection sensitivity and the stiffness we get the normal force pushing on the contact.

$$F_N(V) * DS * k = F_N(nN) \tag{2.4}$$

$$V * \frac{nm}{V} * \frac{N}{m} = nN \tag{2.5}$$

It is important to note that the adhesion force between the sample and tip does not affect the normal force. This is because the tip is pushed down in a closed-loop system. Any change in the normal force because of a change in adhesion force would be nullified by a change in the piezo, keeping the applied normal force constant.

2.5 Lateral Calibration by sloped Grating

With LFM we measure the torsional deflection ($V_{lateral}$) of the cantilever that results from the friction force at tip to surface interface. It is assumed that the lateral deflection is proportional to the friction force [19].

$$F = \alpha * V_{lateral}$$

To calculate the proportionality constant, α, we can either analyze the geometry of the cantilever and system as explained in section 2.6 or perform a calibration measurement. The disadvantage of the geometric solution is a large uncertainty and variation between tips. The calibration method we use is based on the work of Varenberg et al. [20]. Their method is based on the assumption that, at normal forces above the Adhesive force, the friction force scales linearly with the the normal force (F_N). If we move on a sloped surface, the effective normal force is higher when ascending the sloped surface than when descending it. This change in friction force also shows in the voltage plot in figure 2.8b.

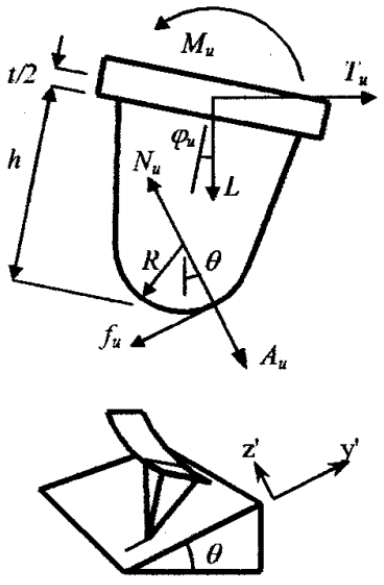

(A) Schematic of the tip as it ascends a slope.

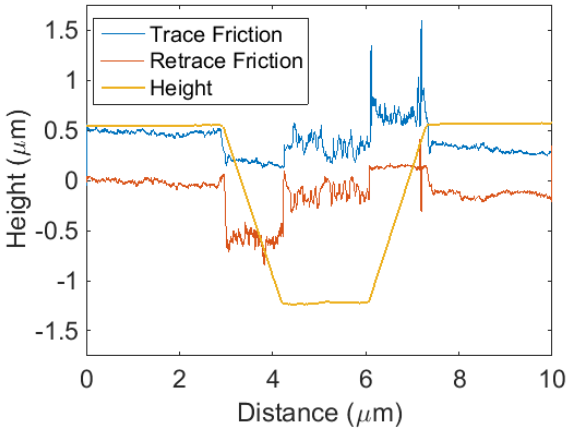

(B) A single scanned line of the grating sample. The yellow is the height profile

FIGURE 2.8

Following the mathematical derivation from Varenberg et al. for sharp tips, tip length larger than tip radius ($h >> r$), they arrive upon (Eq 21 in [20]);

$$sin(\theta) * (L * cos(\theta) + A) * \mu^2 - \frac{\Delta_o}{W_o}(L + A * cos(\theta)) * \mu + L * sin(\theta)cos(\theta) = 0 \quad (2.6)$$

Where Δ_o is the output offset (in Volts), W_0 is the Friction Force (in Volts), L is the normal force (in Newtons), A is the Adhesion force (in Newtons, measured through ramping) and θ is the slope of our grating (which for us is 54.74 degrees). The values we get from the calibration sample are Δ_o and W_o (shown in figure 2.9). W_o is the friction force on the sloped surface, while Δ_o is the corrected offset $\Delta = \Delta^{Sloped} - \Delta^{Flat}$. Sometimes the fraction $\frac{Delta}{W_o}$ becomes so small that we get imaginary solutions. We looked at the option to correct the offset by a linear correction, to get Δ^{Flat} closer to zero, which sometimes solves our problem. However, it is not part of the calibration by Varenberg et al. so we would need to test rigorously whether this will result in the correct calibration factor.

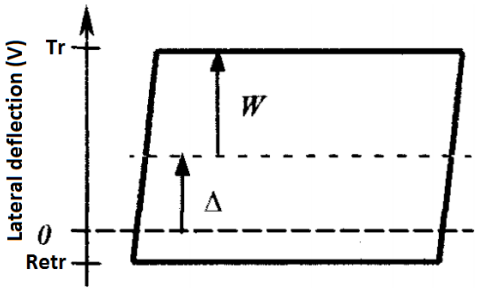

FIGURE 2.9: Schematic torsion loop obtained on a sloped surface. W and D represent the half-width and the offset of the loop, respectively

Clearly the second order equation gives us two values for μ/α. In many cases one of the solution for μ is smaller than $\frac{1}{tan(\Theta)}$ which is impossible as it would result in a negative conversion factor. In the case of two $\mu < \frac{1}{tan(\Theta)}$, *Varenberg* suggests to take the μ which is closest when comparing the sloped and flat result. The flat result is simpler and can be calculated by solving;

$$\mu^{flat} = \frac{\alpha * W_o^{flat}}{(L + A)} \quad (2.7)$$

As μ_{flat} should be approximately μ we take the value which is most consistent. To calculate the proportionality factor α we solve;

$$\alpha = \frac{\mu^2 * sin(\theta) * (L * cos(\theta) + A) + L * sin(\theta) * cos(\theta)}{cos^2(\theta) - \mu^2 sin^2(\theta)} \quad (2.8)$$

We performed this calculation for two tips at different Normal forces, the results of which are shown in figure 2.10. For low normal forces, we have large errors confirming that to have an accurate conversion factor, we need a normal force well above the adhesion force (which was around 700 mV in this case). For the higher normal force, we see a clear horizontal behaviour. Confirming that the conversion factor is independent of the applied normal force.

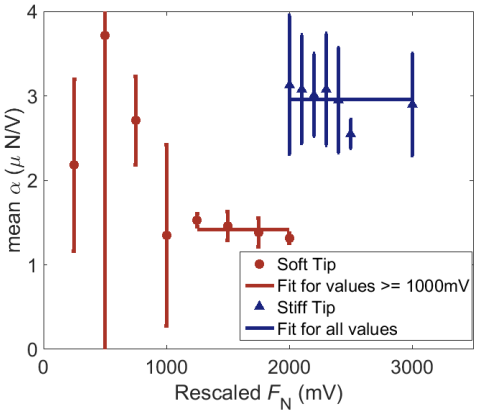

FIGURE 2.10: Two independent sets of Alpha values for varying Normal Forces. The red points are a soft tip with normal stiffness k of 9.4(9) N/m. The blue points are a stiffer tip with normal stiffness k of 50(5) N/m. We measure a constant Alpha value for normal forces above the Adhesion Force (here around 700mV).

2.6 Tips used

AFM tips are generally chosen based on their Resonance Frequency (kHz), Cantilever stiffness (N/m) and tip radius (nm). The Resonant Frequency and the Cantilever Stiffness are directly linked, a softer cantilever will have a lower resonant freqeuncy than a stiff cantilever. The Cantilever Stiffness (k) is the force needed to bend the cantilever a distance m in the normal direction. Because of this we refer to it as the normal stiffness, as opposed to the lateral stiffness, which is the amount of force needed to rotate the cantilever. A low stiffness cantilever will be more likely to follow the surface and so wear less, this is why softer cantilevers are preferred for contact mode AFM. But the soft cantilevers have a low resonant frequency, which is ill suited for tapping mode or Peakforce. To obtain the best approximation of the tip radius, as detailed in the next section, it is preferred to use PeakForce, which is why we switched to stiffer RTESPA-300 instead of the softer ESPA-V2 tips. All details of the used tips can be found in table 2.1.

In the information provided by Bruker there is an uncertainty of almost 50% in the parameters of the tips. This uncertainty results in large errors for calculated normal

[3]https://www.brukerafmprobes.com/p-3895-espa-v2.aspx
[3]https://www.brukerafmprobes.com/p-3907-rtespa-300.aspx

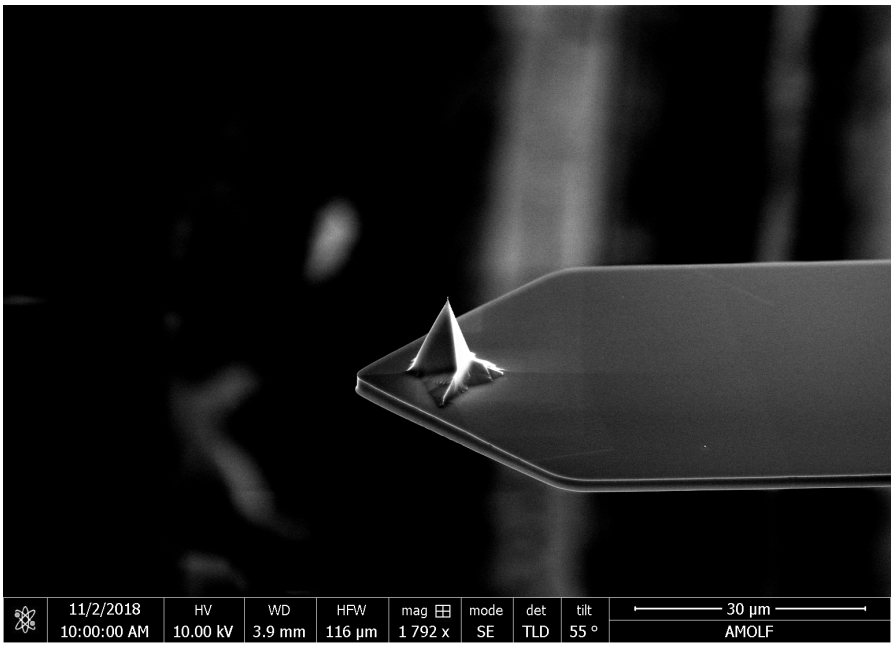

FIGURE 2.11: SEM image of the ESPA-V2 tip as used within this thesis.

and lateral stiffness (shown in table 2.2). This translates to large differences in the results between different tips. We therefore deem it necessary to calibrate each tip to ensure reliable quantitative results. When comparing within one measurement, it is possible to skip calibration steps as the normal and lateral stiffness for one tip placement is within our measurement precision.

Name	Resonant Freq.(kHz)	Stiffness (N/m)	Tip Radius(nm)
ESPA-V2	9(4)	0.2(2)	8(4)
RTESPA-300	300(100)	40(20)	8(4)

TABLE 2.1: Information supplied by Bruker about the ESPA-V2 contact mode tips, and the RTESPA-300 tips which where used in the experiments explained in this thesis. The cantilevers are made of SiN, while the sharp tips are Antimony (n) doped Si.

To calculate the stiffness of rectangular cantilevers analytically, we can use simple mechanical equations. For the normal stiffness this is given by [21];

$$k_z = \frac{E * b * h^3}{4 * L^3} \tag{2.9}$$

Where the E is the Youngs modulus ($169GPa$ or $1.69 * 10^{11} N/m^2$ for Silicon [4]), b is the cantilever width, h is the cantilever thickness and L is the cantilever length. The lateral stiffness is given by [22];

$$k_{lateral} = \frac{G * b * h^3}{3 * L * l^2} \tag{2.10}$$

[4] `https://www.spmtips.com/AFM-probes-faq.afm#6`

where G is the the shear modulus (50 GPa or $0.50 * 10^{11}$ N/m^2 for Silicon [5]) and l is the height of the tip, which slightly changes during the measurement as a result of wear.

If we say that $E/4 \approx G/3$ we clearly see that $\frac{k_{lateral}}{k_z} \alpha \frac{L^2}{l^2}$ where the length of the cantilever is generally a order of magnitude larger then the tip size. This can also be seen in table 2.2, where the torsional Stiffness is respectively a factor 600 and 50 higher than the normal stiffness. This means that in the case of small miss alignment, in which a normal force contribution is measured as a torsional effect, would greatly influence our measurement. We expect that this would mostly affect the offset of the friction loop. When measuring the friction, we look at the difference in trace and retrace, which should not be affected by a change in offset.

Name	Stiffness (N/m)	Torsional Stiffness (N/m)
ESPA-V2	0.18(13)	120(80)
RTESPA 300	34(15)	1.6(8) $*10^3$

TABLE 2.2: The different tip values calculated Analytically using equation 2.9 and 2.10 for the normal and torsional Stiffness respectively

[5] `https://www.spmtips.com/AFM-probes-faq.afm#6`

2.7 Tip Radius by deconvolution

The used AFM tips are extremely sharp, resulting in contacts in the order of tens of *nanometers* or only a few hundred atoms. Because of this, wearing only a small number of atoms will already greatly influence the measurement. In this section, we explain a method to determine the tip size and geometry through deconvoltion with a rough surface. At the end, we will introduce literature which has confirmed the validity of the deconvolution method through direct measurement of the tip by Transmission Electron Microscopy (TEM). For the results of our first approach through Scanning Electron Microscopy (SEM), we refer to appendix A.

The deconvolution method is available and explained by Bruker and official Nanoscope information [6]. To understand this method, it is critical to first realize that the AFM measurement is always a convolution of the sample and the used probe (tip). An example can be seen in figure 2.12a which shows that our resulting image greatly depends on the sharpness of the tip. Interestingly, this convolution effect can be used to measure the tip shape. We simply scan a sample with very sharp peaks and deconvolute the resulting images, as schematically shown in figure 2.12b. It is important to emphasize that by deconvolving we calculate a maximum tip size/radius and not an exact value.

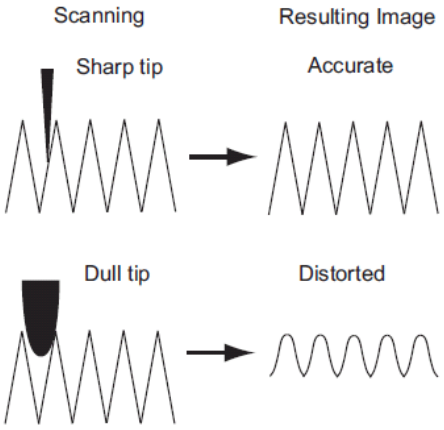

(A) The difference in the measurement of a sharp sample because of a dull tip.

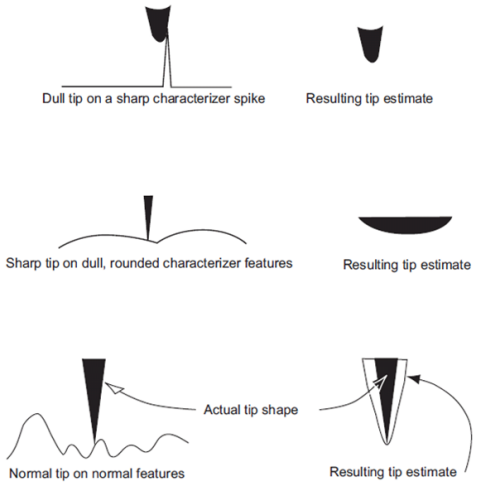

(B) This implies that our tip radius is always a maximum value.

We perform the pre-programmed *Tip Qualification* method by Bruker. As counter surface we use a Titanium roughness sample (RS) [7], which consists of sharp pyramids with ultra-sharp edges. Figure 2.13 is a screen-shot of the method within Nanoscope. In the flattened scan we see the sharp edges of the RS sample. The green points in

[6] `http://www.nanophys.kth.se/nanophys/facilities/nfl/afm/icon/bruker-help/Content/PeakForceQNM/Calibration/TipRadius.htm`

[7] `https://www.brukerafmprobes.com/a-3743-rs-12m.aspx`

the image are the defined peaks that are used to estimate the tip size. Within the Tip Estimation header we can choose certain parameters. The most important part is that we one always uses the same parameters when comparing tip sizes in order to have a reliable qualitative comparison. *Tip image Size* should always be a multitude of the largest tip you have measured. For new tips a 100 nm is large enough while for strongly worn tips (tip radius $\approx$ 50 nm) we need at least 200 nm. *LPF for Max Select* is the Low Pass Filter to exclude artifacts, for very clean images we can turn it off. As our tip becomes bigger we get more artifacts and it is necessary to use the LPF. In combination with *Sigma Multi for Spike Rejection* we can change the variable to get a continuous tip estimation. The higher you make the values, the more you will overestimate the tip size.

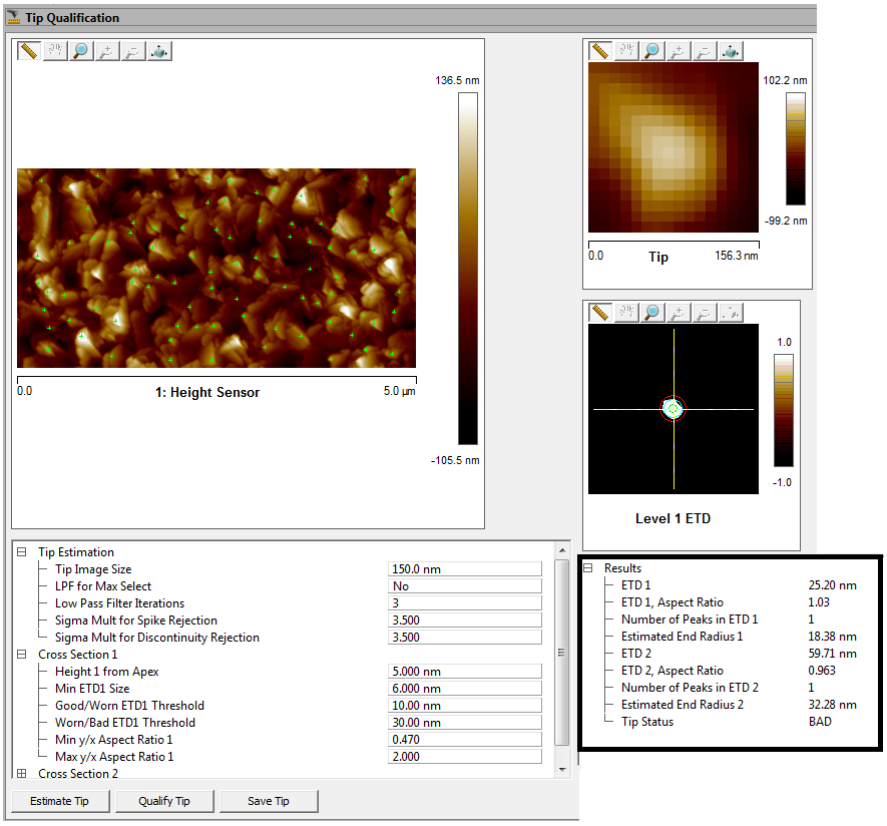

FIGURE 2.13: Example evaluation through the Bruker Tip Qualification

We can also save the estimated tip for further analysis. With matlab we can plot a three dimensional visualization of the tip. Figure 2.14 shows a before and after image for an ESPA-V2 tip, with the same axis. We can clearly see that the tip has become rounded. This increase in tip radius likely results in an increase in area of real contact between the tip and a flat substrate.

To test the dependability of the method, we checked multiple new and worn tips (table

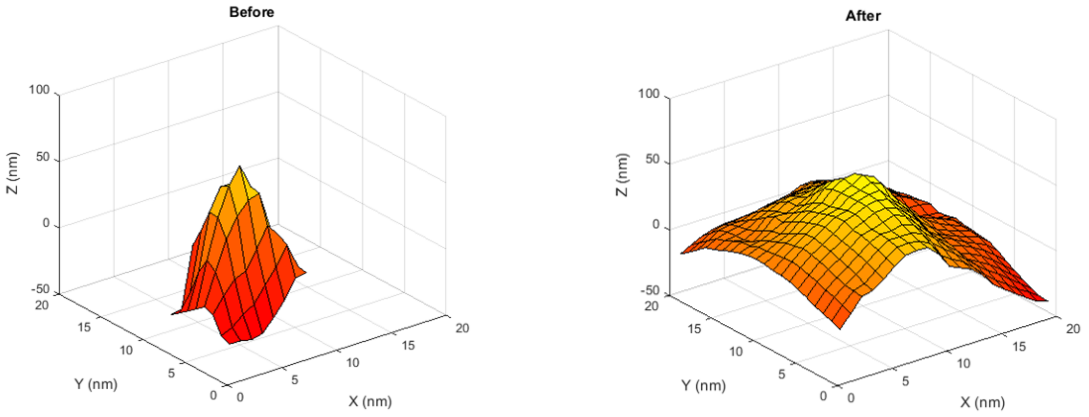

(A) new ESPA-V2 tip (B) ESPA-V2 tip after use

FIGURE 2.14: The tips used for the wear experiment in appendix D, presented in 3D with the same axis so we can clearly see dulling of the tip.

FIGURE 2.15

2.3) measuring an order of magnitude difference in the measured tip radius. An alternative approach to evaluate the tip radius directly is by using Transmission Electron Microscopy (TEM), as was shown by *Jacobs,Chung and others* [23] [24]. As the TEM has a higher resolving power, it can capture the subtle changes in tip geometry [25]. The high vacuum inside a TEM protects the sample from carbon deposition as observed within the SEM (appendix A). This method is generally difficult and intrusive compared to measuring within the AFM. This leads us to conclude that, unless sub *nanometer* precision is required, tip radius through deconvolution is the preferred method. Recently Flater et al. [26] have confirmed the reliability of the deconvolution method by comparing its results with direct TEM measurements. Furthermore, the deconvolution method was also used by colleagues at the VU to evaluate tip wear, giving comparable results as we presented [27].

Name	Radius new tip (nm)	Radius worn tip (nm)
ESPA-V2	7(3)	45(5)
RTESPA 300	3(2)	45(5)

TABLE 2.3: Comparing the found apex tip-radius for new and word tips calculated thorugh the deconvolution method.

The ability to measure the tip radius within the machine also allowed us to measure wear of the tips. The process of tip-wear is extremely interesting because it changes our measurement over time. It can also be relevant for the ASML application because if we can reduce wear of the asperities in the nanolithography system, this would improve the stability of the wafer-on-wafertable friction force over time (application of this is shown in appendix D). And finally, by understanding the process of nanoscale wear, we would be increasing our fundamental understanding of the asperity to surface interaction.

2.8 Fast Fourier Transform (FFT) for oscillations

To find external noise in our data we use the Fast Fourier Transform (FFT). FFT deconstructs our measurement in its oscillating parts. Relevant is that if the observed oscillation is sample dependant it is always the same size, while if it results from an external source the size depends on the data acquisition speed. Figure 2.16a shows the retrace of a force loop. Figure 2.16b is the FFT of the second 75% of the retrace. We do not take the first 25% into account as it is an effect of the static friction. The presented FFT in figure 2.16b is very irregular. To diminish this noise we take multiple lines (either 16 or 32 is fine, depending on the required precision/speed). We take the FFT of each individual scan line and by averaging all FFT spectra we get a smooth curve, with clear peaks (Figure 2.16c). The FFT procedure (pre-programmed in Matlab [28]) gives the frequency of an oscillation per line. To transform this into an actual frequency, we need to divide the FFT-frequency by the time used to scan a single line. Notice that we only use the trace so it is $\frac{1}{2*ScanRate}$ because within one 'Scan Rate' the AFM measures both trace and retrace.

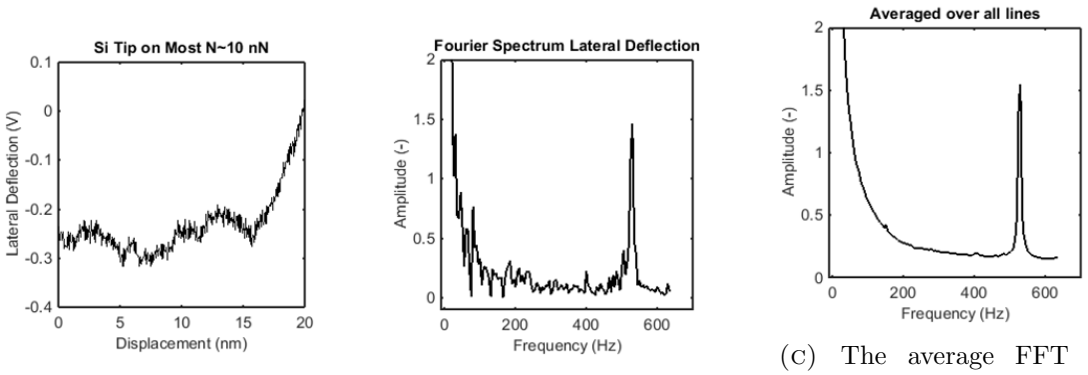

(A) The Retrace of a Single Friction Loop.

(B) Fast Fourier Trasform (FFT) of a single line.

(C) The average FFT of 32 Retrace friction measurements.

FIGURE 2.16: Example of the FFT process

By comparing the FFT-spectra of two measurements with different scan-rates, we can see whether an oscillation is external in nature or the result of periodic height differences in the sample. The principle is that external influences would always produce the same frequency, while the frequency of periodic change in the sample would depend on the scan-rate. Figure 2.17 is an example of a found external vibration.

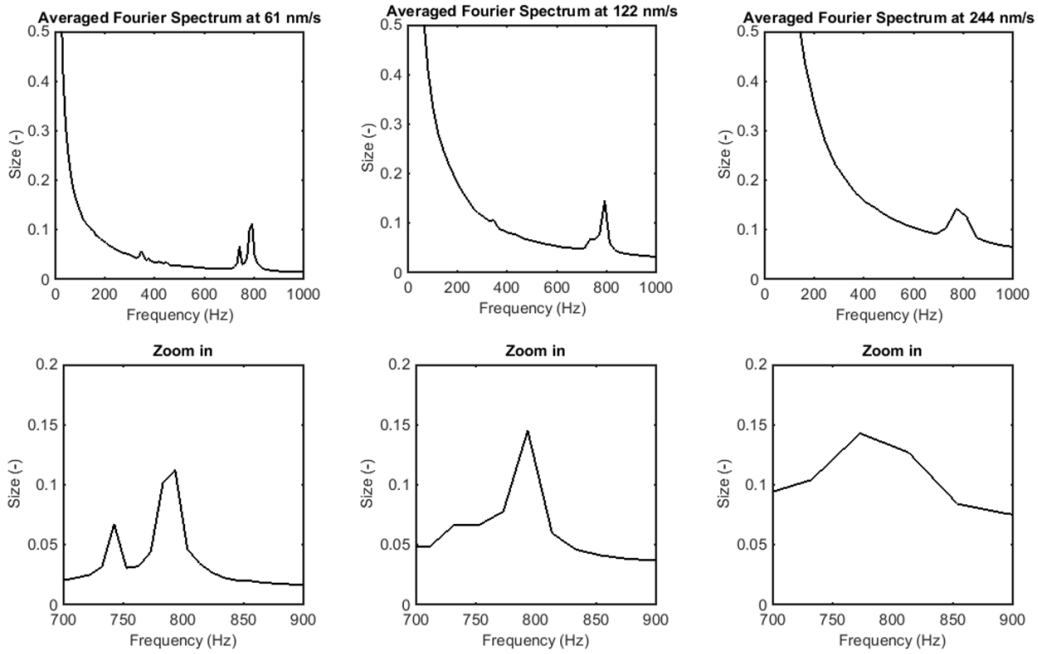

FIGURE 2.17: Scans done with VESPA-V2 tip, 512x512 lines, 6x6 nm

Using this method, we found a strong external vibration at 780(30) Hz. We expect this vibration to be because of the pump of the chuck vacuum. The vacuum is used to clamp the stage down when the tip engages. Any instabilities in the created vacuum would create vibrations in the stage. Furthermore, the chuck vacuum can be used to clamp the sample to the stage. We tested that the vibration increases when we use the chuck vacuum to clamp our sample. This further strengthened our believe that the vacuum pump was responsible.

Chapter 3

Friction through coupled phonons

To understand friction it is critical to correctly define the effect called friction. Often we represent friction as a force which acts against movement. It pushes against any moving object, slowing it down and reducing it's energy. We also see this if we look at the units of force; $Newton = Energy * meter^{-1}$. So essentially *Friction force* is a measure of energy lost per distance. For the proposed model it is important to understand friction as an effect which siphons energy from a moving system instead of a counter force.

We start with a theoretical system of an atomically sharp tip sliding over a periodic crystalline surface (figure 3.1). The crystalline surface creates a periodic energy potential landscape, with potential barriers representing the atoms, while the minima are exactly between them. As the tip moves up from a minimum to a maximum there is an increase in the potential energy of the system. This energy has to be supplied and we observe this loss of energy as friction. As the tip continues over the energy barrier it moves down into the minimum, releasing potential energy, which should generate a negative friction force. We would expect a force pushing us forward, making our total observed friction zero. This clearly does not stroke with reality; an important element is missing and to understand what this element is, we need to consider single-asperity experiments.

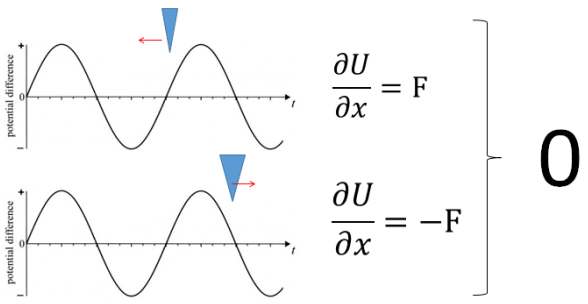

FIGURE 3.1: Schematic of theoretical tip over the potential energy landscape.

Figure 3.2 shows *stick-slip behaviour*, a saw-tooth like pattern that is often observed in friction experiments [29]. The friction increases as the tip climbs the potential maximum. Yet at the maximum, instead of returning this energy in the form of negative friction, the friction returns to the same starting point and all invested energy is 'instantaneously' lost. The commonly used *Prandtl–Tomlinson model* [30][31] simply assumes all energy invested lost and dissipated, but it does not explain how the energy was dissipated.

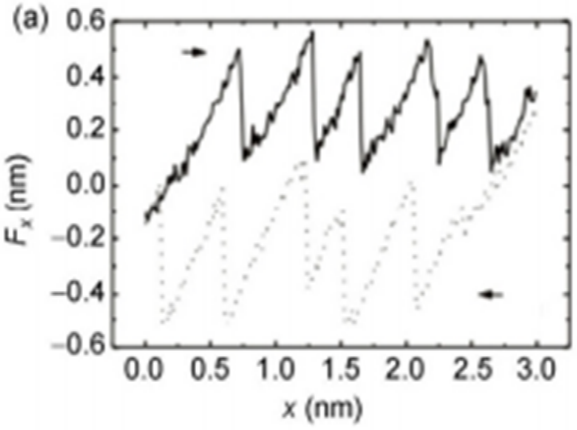

FIGURE 3.2: Example of Stick slip motion made within a ultra high vacuum LFM [29]

Yet it is by understanding how the energy dissipates that we hope to understand the fundamental cause of fiction and can suggest avenues to control it. Within this chapter we will introduce a novel theory developed by Professor Frenken[1] and Professor Krylov[2][8] and propose an experimental method to test it.

3.1 Phonon de-phasing

The fundamental two requirements our model has to satisfy is that it should dissipate the kinetic energy and it has to do so in short times scales, so that it would experimentally be considered instantaneous[32]. The presented theory ascribes energy dissipation in friction to the de-phasing of phonons. Phonons are quantized mechanical vibrations within the crystal. Their quantum mechanical nature indicates that they are global and have fixed quantized energies.

Figure 3.3 a) shows a cartoon of how the overcoming of the energy barrier displaces the underlying atom. In b) and c) we see how this local displacement can be described as a set of global eigenstates. In the macro-scale there are an infinite amount of possible phonons so the approximation would be exact.

[1] University of Amsterdam and ARCNL
[2] Russian Academy of Sciences in Moscow

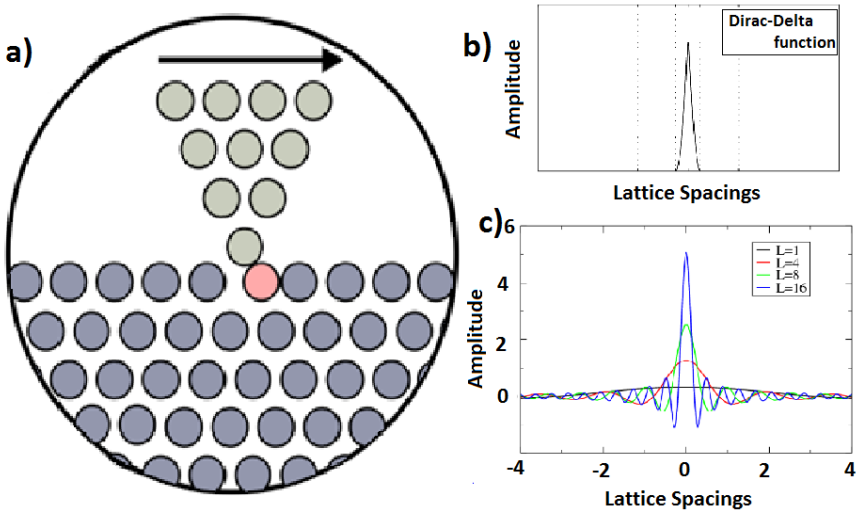

FIGURE 3.3: (a) The displacement of one atom is a localized effect. (b) A localized effect can be described by a Dirac delta function. (c) Such a localised interaction can be approximated by a sum of global sinuses; already with 16 sinuses (blue line) do we approximate a localzed dirac-delta interaction.

As long as the tip pushes against the potential barrier the excited atom is kept in place and all phonons are stationary. As the tip passes the energy barrier, all phonons are free to oscillate. As each phonon has a different oscillation frequency, they quickly de-phase. They no longer correlate to a strong displacement but the different maxima and minima cancel each other. Figure 3.4 shows the total displacement and shows that after a single oscillation the effective displacement is negligible. This dephasing happens on much shorter time scales than the conventional energy dissipation, so fast that to any current experimental method it would be considered instantaneous. Important to note is that the energy is still in the system but unavailable to overcome the next energy barrier. The dephased phonons will continuously be lost to the system through phonon scattering [33] till all energy is thermalized and the kinetic energy turned to an increase in temperature of the system. This process typically takes much longer than the damping observed in either experiment (Figure 3.2) or the presented theory (Figure 3.4).

We have presented a description of how the sliding motion is damped and that it does so within shorter time spans than we can experimentally probe. By limiting the amount of phonons available to dissipate the energy, we can lengthen the damping time, allowing us to experimentally test our theory. As the phonons are eigenstates of the crystalline structure we can limit them by limiting the available atoms in the system. If less phonons can distribute the displacement they also need more time to dephase, which means that the invested energy will be available to overcome the next potential barrier. A second hypothesis is that as the amount of available phonons becomes , the amount of energy they can maximally represent also becomes limited. This quantum mechanic

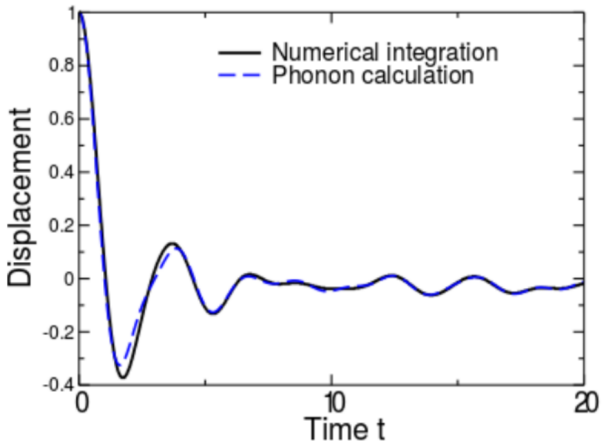

FIGURE 3.4: Here we see the damping of the total deplacement as a result of phonons dephasing. We see that after one oscillation the displacement is already critically damped.

interpretation would even suggest that if the finite amount of phonons cannot absorb the energy, it cannot be lost.

Possible experimental confirmation of this limited size effect came in spring 2018 in an article by Wada et al.[9]. They measured a sharp decrease in friction for square islands smaller then $1\mu m^2$, even reporting a decrease in friction of up to a factor 80 for islands of 200x200nm. For this thesis, we have tried to reproduce such behaviour for various materials and parameters.

3.2 Previously conducted Phonon Confinement experiments

An article from April 2016 by Wada et al.[9] shows a sharp decrease in energy dissipation by limiting the amount of interacting atoms. Wada et al. fabricated islands on MoS_2 using FIB milling. MoS_2 is part of a group of transition metal dichalcogenide (TMD) monolayers which are characterized by the MX_2 structure where M is a transition metal atom (partial filled d-shell) and X a Chalcogen atom (column 16 of the periodic table, same as oxygen and Silicon). Each layer of Molybdenum is in between two layers of Sulfide, giving rise to a weak transverse interaction. Thus the interacting atoms are limited to those in the plane giving rise to 2-dimensional behaviour. They made square islands of varying size as seen in figure 3.5 a). The most relevant result (figure 3.5) was local friction measured on the islands through lateral force microscopy. They report a correlation between friction and island size over multiple orders of magnitude. Reporting a decrease of almost two orders of magnitude between friction on a 200x200nm island and bulk material. They also mention that they observed a comparable change in friction for speeds between 60 to 1000 nm/s and normal forces of 1 to 100 nN.

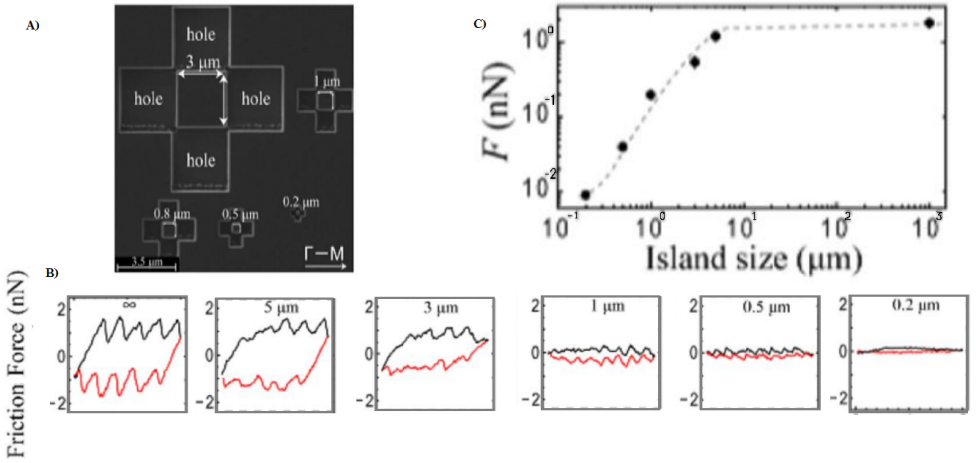

FIGURE 3.5: Results from Wada et al.[9]: friction measurements done with scans of *2 nm* at *100 nm/s* and *1 nN* Normal Force.

Wada et al. theorize that the effect they measure is because of acoustic phonons. Acoustic phonons are coherent movements of atoms of the lattice out of their equilibrium positions. As acoustic phonons propagate over the surface, Wada et al. hypothesize that in the case of a limited system they would be reflected at the islands edges. This would keep the generated acoustic phonons at non-equilibrium and confined within the island. But we believe that this could not describe macro-scale friction, because if these acoustic phonons would lubricate the contact this would also apply to macroscale systems. In this case the acoustic phonons of different single asperities would lubricate each other. Instead we hypothesize that the decrease of friction happens because of the phonon confinement. Because of limited number of phonons the damping time is extended. This allows the invested energy to be re-used to overcome future energy barriers, resulting in a decrease of friction.

3.3 Sample preparation by Focused Ion Beam milling

To investigate the relation between friction and the geometric confinement of phonons, we created two dimensional islands by Focused Ion Beam (FIB) milling. By exposing specific parts of the surface to a high energy ion beam we locally remove atoms from the substrate. The exposed atoms absorb part of the momentum of the incoming ions. This energy causes them to move away from the surface. Through FIB we can make patterns as small as 10nm laterally[34]. The ions with which the FIB bombards the substrate are inert elements to limit the effects of implementation. In our case we used Gallium ions.

For FIB we made use of the Helios FIB from the AMOLF Nanolab[3]. An important aspect of this system is that it contains both a FIB and a SEM setup (see appendix A for more information on SEM) so it is possible to make high resolution images of the created structures. The islands are made by milling out squares around them. Figure 3.6 shows an example of three $1\mu m^2$ islands, of *100nm* height, created and imaged within the FIB.

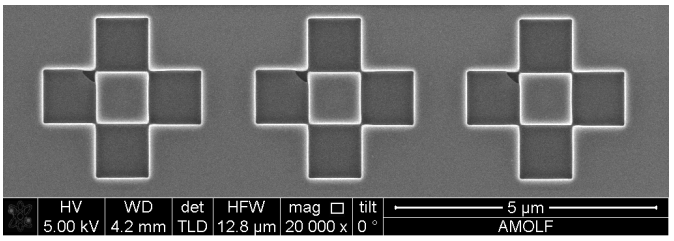

FIGURE 3.6: Three 1x1um islands made by FIB-milling.

For all presented island heights it is important to note that the depth has been calibrated for crystalline silicon, so we can assume a relatively well defined depth for the islands on the wafer. But the depth can have a large deviation for other materials like the MOST sample presented in section 4.3.

[3] `https://amolf.nl/fei-helios-nanolab-600`

3.3.1 Scale up to UMT experiment

We have investigated how to increase the area covered by islands and whether this would allow us to manipulate macroscale friction. Specifically, whether we could restructure the contact area of a sphere for use within the UMT. By covering the contact point with a checkerboard structure (figure 3.7), our contact would be a multitude of many size limited contacts. The first problem here is that it is hard to define exactly where the contact point of a spherical contact is within the FIB. Our solution is to first make a short run in at the UMT to define the contact point. The second problem is that the FIB mills point by point which takes a long time if we want to cover the complete UMT contact point. The time taken to burn to a specified depth depends linearly on the ion beam energy, but the resolution depends inversely on the energy of the ion beam. So if we increase the beam energy we would limit the necessary time but lose resolution. If we want to make multiple macroscale samples lithography may be a better method. We could create a mask by FIB or Electron-beam configuring. Then we can use lithography to make multiple samples using this one mask.

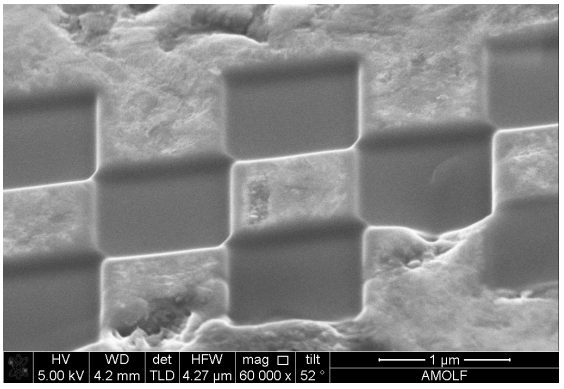

FIGURE 3.7: Checkerboard structure for covering large contacts on a MOST sample.

Chapter 4

Lateral Force Microscopy on nano-patterned surfaces

In this chapter, we present our measurements done on size limited systems, created by FIB as described in section 3.3. As explained in chapter 3 we predict that nano-structures produce a lower friction than bulk material. As our system becomes smaller we limit the number of interacting atoms, which limits the possible phonons. A limited amount of phonons is less efficient at distributing energy, thus less effective at dissipating energy, resulting in a lower friction. We measure the friction by *Lateral Force Microscopy* (LFM), where we bring an AFM tip in contact with our relevant surface measuring the torsion of the cantilever induced by friction. Further details on LFM, including calibration, can be found in chapter 2.

4.1 Islands on Silicon Wafer

To investigate whether we can control friction by creating a size limited system we created islands on a flat silicon [100] wafer. We used silicon because it is a well-understood system with very precisely defined parameters. Furthermore, as silicon wafers are the basis to the nano-lithography process we can be assured that the results obtained can be applied to the processes at ASML.

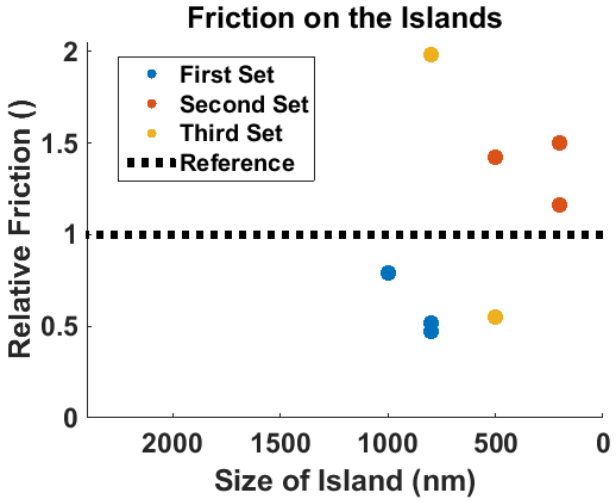

FIGURE 4.1: Plot of the relative frictions of our first sets of island measurements. We chose to use relative friction to diminish the influence of calibration errors. Each set was measured on a different day and with a different tip.

Figure 4.1 shows an overview of the first measurements on square silicon islands. We plot the normalized friction on the islands compared to the friction on the bulk ($F_{Relative} = \frac{F_{Island}}{F_{bulk}}$), such that the result is dimensionless and any uncertainty about the calibration no longer relevant. The dashed line at *1.0* shows a reference for which bulk and island have the same friction. We see that, although the first set of measurements shows a decrease in friction with decreasing island size, the results from the three sets taken together does not support such a trend.

To more rigorously test the system, we performed a large amount of smaller scans within one large set. This means that the tip was not changed, nor was the photo-diode recalibrated, between the measurements. Figure 4.2 shows these smaller scans. Again we observe no decrease in friction on the islands compared to bulk properties. If we look at the average values (given in the inset), we see a small overall decrease in friction, but this decrease is much smaller than our uncertainty. We do see that the measurements on the bulk are reproducible, implying that at these parameters we have minimal influence because of wear.

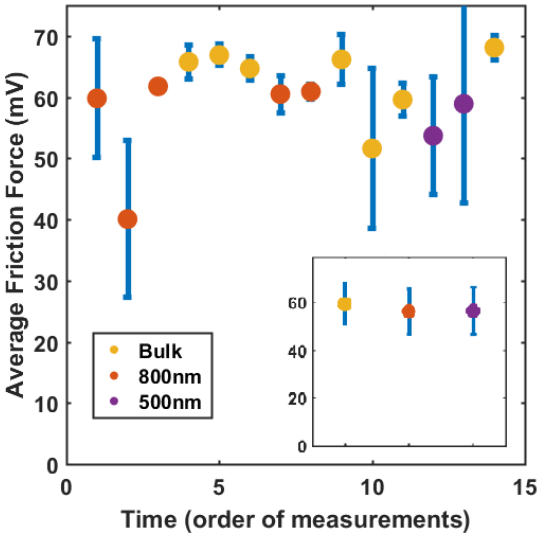

FIGURE 4.2: Plot of the friction force at different locations. Every presented point is the average of 4 measurements of 10x10nm done 100nm away from each other at 100 nm/s. The measurements are presented chronologically where the most left was done first and the most right last. The inset shows the average values.

Silicon has both a lateral surface interaction and a perpendicular bulk interaction. If this strong perpendicular behaviour affects our system, the energy will be dispersed not only over our surface atoms but also the deeper atoms. In the case of such a three-dimensional system, the depth of the trench around the island is an important parameter to suppress the energy dissipation. We present the results from testing this hypothesis in section 4.2.

4.2 Islands with different depth

Islands with varying height were made in a new clean silicon wafer through FIB, as explained in section 3.3. In figure 4.3 we compare the friction on 1x1 μm islands with different depth trenches around them, resulting in different effective heights for the islands. Each measurement point is the average of four measurements with the error one standard deviation.

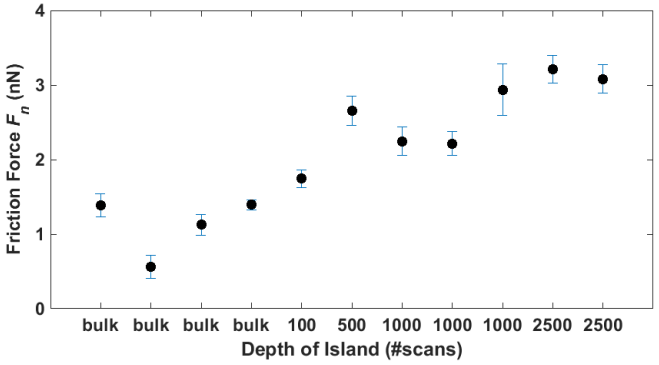

FIGURE 4.3: Friction for 1x1 μm islands of different heights. All scans were done with a single RTESPA tip, line density 4096 for 30 lines of 50 nm each, at 100 nm/s and a normal force of 2700(300) nN.

Instead of a decrease in friction as the islands become higher we actually measure an increase in friction. This increase in friction also correlates with time as we started with the shallowest island and subsequently moved to the higher ones. To test whether this change could due to some time dependent change, we have done follow up measurements presented later in this section (figure 4.6).

We also investigated the stiffness of the interaction between the tip and the surface on different height islands, which is presented in figure 4.4. This stiffness does not appear to increase with time. If we exclude the two outliers (data point 2 and 7) we are left with a reasonable constant stiffness of .75(17) N/m (0.75(9) N/m without outliers) over the measurements. It is important to note that this stiffness is close to 1 N/m, after taking the lateral stiffness into account. A stiffness of 1 N/m corresponds to the expected value for an atomically sharp interaction [35] [36]. We also investigated whether there would be a correlation between the change of friction and the effective stiffness of the contact, presented in figure 4.5a.

The correlation in figure 4.5a is unclear, pronounced by the low R-square value of 0.29. If we exclude the largest outliers (figure 4.5b), we get an R-square of 0.87, which is a significant correlation, but we need to further investigate why these points deviate. If the observed increase in friction was not because of the increase in stiffness, it might be

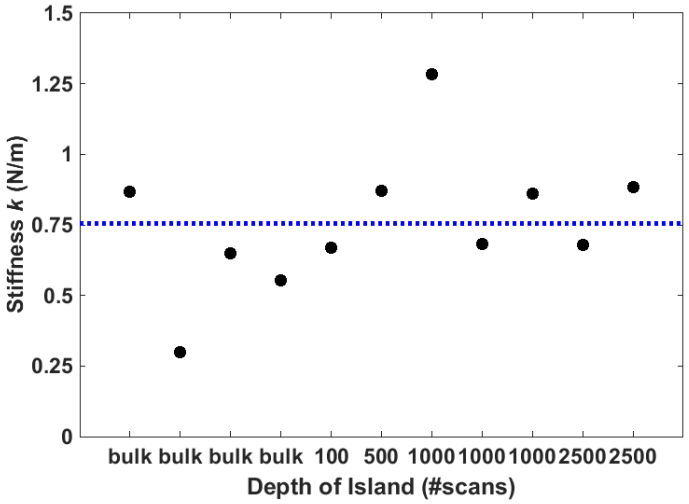

FIGURE 4.4: Stiffness for 1x1 μm islands of different heights and the bulk. The average value, blue dashed line, is 0.75(17) N/m. All scans were done with a single RTESPA tip, line density 4096 for 30 lines of 50 nm each, at 100 nm/s and a normal force of 2700(300) nN.

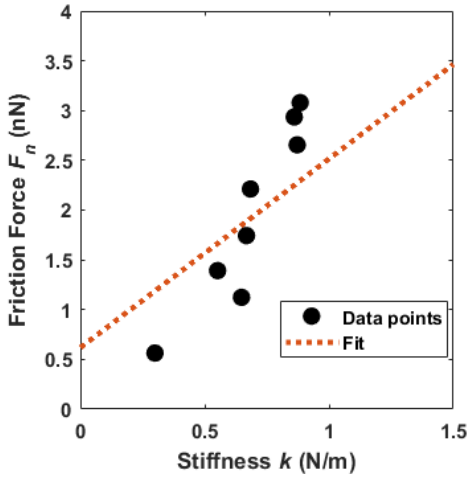

(A) The fit has a slope of 1.9 (nm) and an offset of 0.62 nN, which is effectively 0. The fit has an R-square of 0.29 .

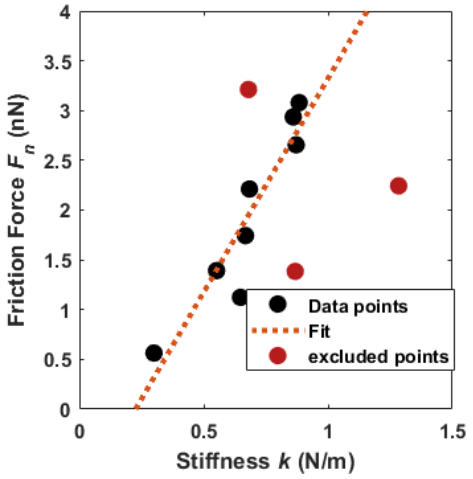

(B) The fit has a slope of 4.3 (nm) and an offset of -0.97 nN, which is effectively 0. The fit has an R-square of 0.87 .

FIGURE 4.5: Correlation between the friction and the interaction stiffness. All scans were done with a single RTESPA tip, line density 4096 for 30 lines of 50 nm each, at 100 nm/s and a Normal force of 2.7(3) μN.

because of the change of height of our islands. To test this, we repeated the measurements done on the 1x1 μm islands, but after measuring the islands in increasing order we also measured them in decreasing order, to test whether this increase in friction was due to geometry or wear. The measurement was repeated on 500x500 nm islands of varying height, at a lower normal force to prevent destruction of the islands. The results (figure 4.6) show a small increase in friction with island depth, but not significant compared to the deviation between measurements. Especially for the 500x500 nm islands we also got

higher values for 100 nm high island.

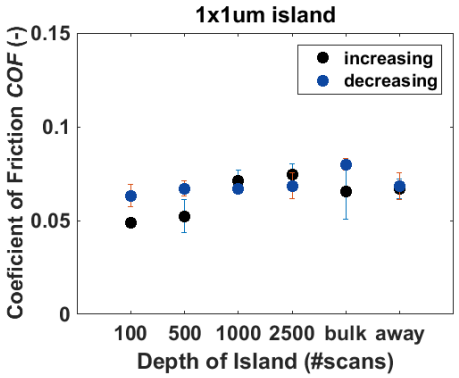

(A) Coefficient of Friction on 1x1 μm islands at 1 V normal force.

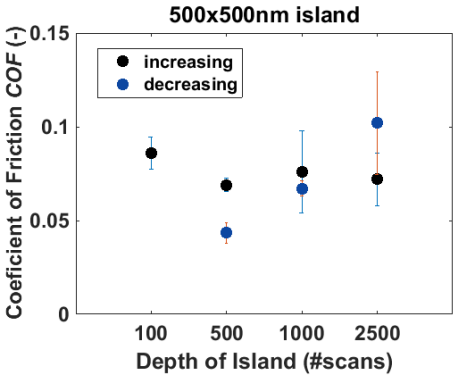

(B) Coefficient of Friction on 0.5x0.5 μm islands at 0.2 V normal force.

FIGURE 4.6: Measurements of the fiction of islands at different depths. To rule out the effect of wear, the measurements were first done by going to increasing higher islands and then subsequently the same islands where measured in order of decreasing height.

Whether the change in friction with changing depth is significant stays a point of discussion. This could be because the sizes we need to look at with crystalline silicon are much smaller then what we are able to measure. This possibility is discussed in more detail in section 5.2. Perhaps by switching to a layered system, like the MoS_2 used by Wada et al.[9], we might observe the effect of phononconfinement at larger islands.

4.3 Titanium infiltrated MoS_2 (MOST)

To limit the number of atoms, and subsequently the number of phonons which are available to dissipate the friction energy, we made a layered sample with weak interaction between the layers. We used a 3 mm silicon carbide sphere with a 500 nm thick Molybdenum di-Sulfide Titanium composite (MOST) coating [37]. This sample was chosen because it was the material closest to the Molybdenum di-Sulfide (MoS_2) that Wada et al. [9] used in their research as presented in section 3.2. As well as that the MoS_2 in the coating has a preference for a layered structure. The sphere was worn by rubbing over a silicon wafer for 1 meter within the Universal Mechanical Tester (UMT), creating a flat surface. We are sure that we have not worn through the MOST coating. All the wearing was done with strokes in one direction, because of this we expect that the resulting surface will have one defined orientation.

Figure 4.7 shows a full set of measurements on bulk and islands, including two spherical islands which were detached from the bulk by a 1 μm wide trench, on the MOST sample. Again we do not observe a decrease in friction for the islands compared to the bulk. But we do observe a factor 30(3) difference in friction between the lowest and highest value.

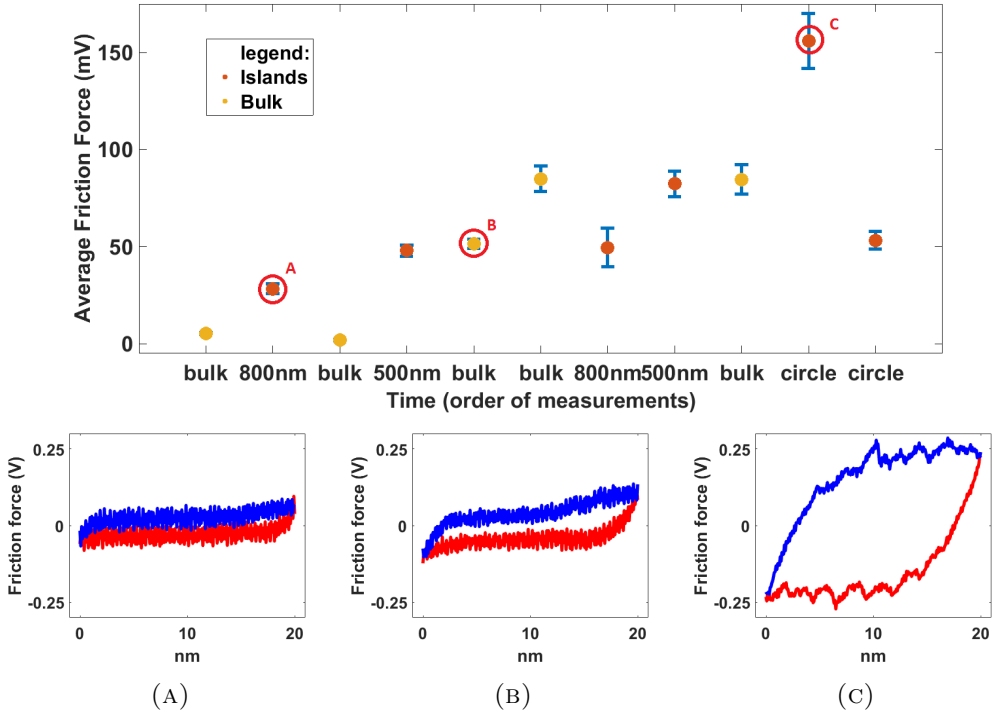

FIGURE 4.7: Friction measurements on MOST. The measurements are presented chronologically where the most left was done first and the most right last. The locations below are the size of the square islands. The circles had a diameter of 1 μm. All scans were done with a single ESPA-V2 tip with line density 256 and 256 lines of 20 nm at 100 nm/s and a constant normal force.

In figure 4.8a we show the effective stiffness of the tip surface interface. Figure 4.8b shows the stiffness versus the friction and we can clearly see a strong correlation. Why an increase in stiffness results in an increase of friction is not trivial, as there are even theories that imply that this should decrease friction [36]. The second question is why the stiffness changes over the course of our measurement. One option is the effect of tip wear, which we discuss in section 2.7 and appendix D, but this increase of a factor 30(3) is many times bigger than we have observed in these dedicated wear experiments. Furthermore, the tip before measurements had a measured tip radius of 3.4 nm and after the measurements, this had only increased to 4.1 nm: an increase far too small to account for such a large change in friction. A second option is that we are creating MoS_2/MOST flakes and that these act as a third body, lubricating the interface. This change in the interface could also explain the measured change in effective stiffness.

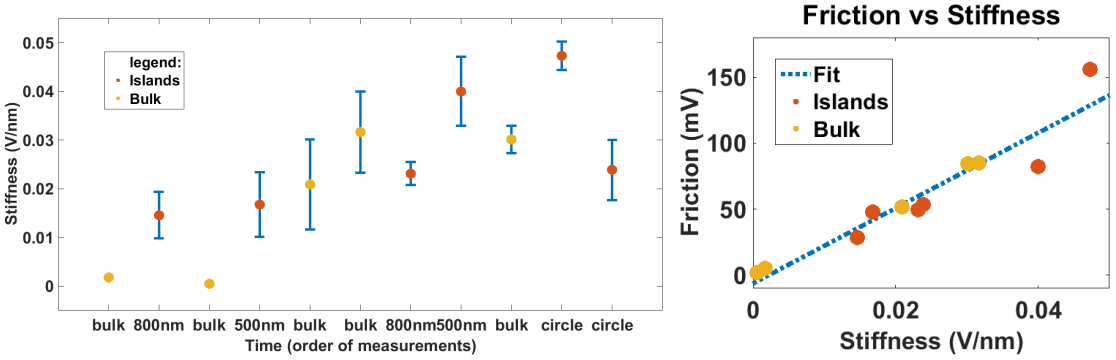

(A) (B)

FIGURE 4.8: (A) Stiffness measurements on MOST. The measurements are presented chronologically where the most left was done first and the most right last. The x-axis give the sizes of the square islands. The circles have a diameter of 1 μm. (B) Correlation of Friction with Stiffness. The linear fit has a slope of 2.85(20)nm and an offset of -6(8)mV, which we assume should be zero. The fit has an R-square of 0.905
.

In figure 4.9a we present the adhesion measurements done on the islands. We plot the correlation between friction and the adhesion force in figure 4.9b. The change in adhesion is a magnitude smaller than the change in friction. Furthermore, there is no clear correlation, affirmed by the low R-square of 0.228 for a linear fit.

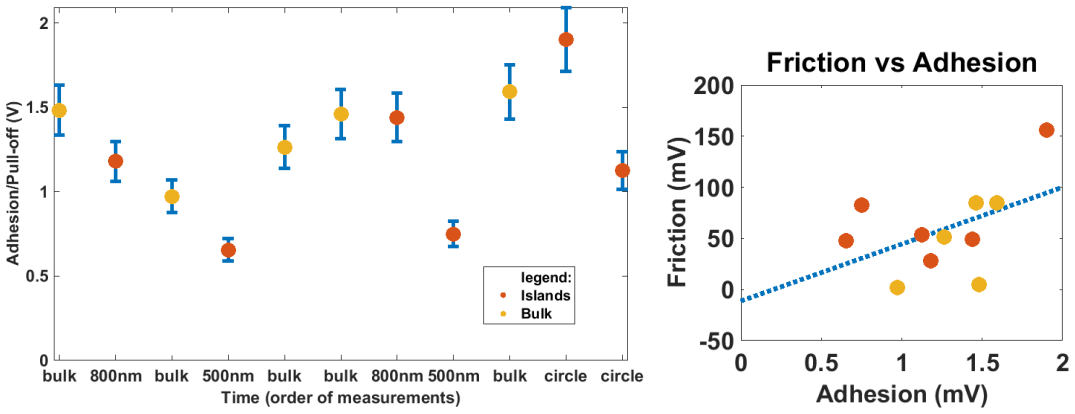

(A) (B)

FIGURE 4.9: (A) After each friction measurement presented in figure 4.7, we measured the Pull-off force through ramping. The ramps were performed at 100nm/s approach and retract speed. With 100mV trigger threshold, which corresponds to 4.0(8)nN normal force. (B) Correlation of Friction with Adhesion Force. The linear fit has a slope of 55(35) and an offset of -11(50). The fit has an R-square of 0.228

We must conclude that the measurements as presented in this section do not imply an island size dependence of the friction. We do observe a large change in friction between our measurements which correlates with the interaction stiffness, perhaps showing direction in explaining the change in friction.

Chapter 5

Discussion

In the discussion we will first discuss the steps made in the method of *Lateral Force Microscopy* (LFM) as presented in chapter 2. Afterwards, we will discuss the principle and results of phonon confinement as presented in chapters 3 and 4.

5.1 LFM measurements

We have investigated how to use *Lateral Force Microscopy* to investigate single-asperity fiction and wear effects. All our understanding and findings of the method are gathered in chapter 2. Our first and foremost challenge was to understand how to control the AFM on a high precision scale. The first step was the normal force calibration. In many scientific reports, the reported normal force is the externally applied normal force [38][39]. This means that their actual normal force is a combination of this applied normal force and the adhesive force. We now know that in our setup the adhesive force is already included in the set normal force, as the deflection setpoint is kept constant by a closed-loop system.

As the set normal force was still in voltage, we needed to calibrate the normal stiffness and the deflection sensitivity. Clearly, the normal stiffness analytically calculated was unsatisfactory precise for our application, as it had an error of either 50% or 80%. Instead, by thermal tune we get a system-specific stiffness which shows only a small change over time. However, it remains unclear how precise this stiffness is. One source of error is the unknown exact temperature of the cantilever. A small deviation in temperature would result in a few percent error on the measured stiffness. In the new version of the NanoScope software we can use two different methods to calculate the normal stiffness. From our first few tests with the new software we observe a difference of around 25% in

the calculated stiffness. This difference might imply that we have underestimated our error in normal stiffness, and subsequently normal force, in this project.

For the deflection sensitivity the ramping procedure is the golden standard and provided us with consistent results. Furthermore, the ramping procedure also allowed us to measure the Adhesion force. Interestingly we observed an increase in adhesion force with larger trigger threshold, while in literature often no direct adhesion force dependence on the loading force is reported [40]. One option is that as we increase the loading force we are also increasing the time the tip is in contact with the surface. This has been shown to slightly increase the adhesive force [41].

Through the Lateral Calibration we have obtained measurements in absolute observables. We have shown that these results are consistent over a range of normal forces, as long as they are above the adhesive force. Furthermore, the combination of normal and lateral calibration allows us to measure the Coefficient of Friction ($COF = \frac{F_{friction}}{F_{normal}}$), which we can compare with macroscopic experiments.

The development of a method to measure the tip radius within the AFM through deconvolution has opened a path in performing nano-scale wear experiments. Some prudence is required when using the tip radius measurements to quantify wear. Firstly, we would like to emphasize that we measure a maximum size of our tip, implying that the actual size of our interaction is always smaller than our estimation. To better understand how large this difference is, it would be prudent to compare some tips through Transmission Electron Microscopy (TEM). Secondly, there is still some freedom in the fit parameters which give different absolute wear rates. Our method is suitable for qualitative comparison.

During our measurements we were greatly hindered by external noise in the data. This has led us to develop the Fast Fourier Transform data analysis method as described in section 2.8. Nonetheless, even with this interference we have been able to show dependencies over much larger ranges than the external error. Furthermore we have been able to show reproducibility of both normal and lateral calibration well within uncertainty.

5.2 Phonon confinement Discussion

The main question of this research project was the origin of adhesive friction in a single asperity contact. In chapter 3 we have presented a phonon based theory of how the energy lost to friction can be dissipated in time scales which would be considered instantaneous to current experimental techniques. As a consequence of the delocalized nature of the phonons, we can predict a decrease in friction for nano-patterned systems. The results from Wada et al. presented in section 3.2 are an indication that the phonon based theory could be correct in describing nanoscale friction.

The results presented in chapter 4 show that we were not able to reproduce the strong dependence on island size that Wada et al. reported. The main difference between our systems was the dimensionality of our samples. For the islands of crystalline silicon, we are sure that our system is 3-dimensional, which greatly increases the number of available atoms and so the number of existing phonons to dissipate the energy. It was because of this effect that we investigated whether higher islands would allow us to measure a decrease in friction, as this would decrease the number of available atoms. But for these measurements we again observed no decrease in coefficient of friction for the islands compared to the bulk material. If we assume an inter-atomic distance (a) of *0.3nm* then 1000x1000 nm is 3300x3300 atoms or about 10^7 atoms. If we take a half-sphere for 3D we get $10^7 = \frac{1}{2} * \frac{4}{3}\pi * R^3_{interaction} \implies R_{interaction} = \sqrt[3]{(\frac{3}{2\pi} * 10^7)} \approx 370$ or about *110 nm*. So we would need a freestanding 3d system of 110x110x110 nm to get the same amount of interacting atoms as we have for a two-dimensional 1x1 μm system, which was the biggest size for which Wada et al. reported a decrease in friction.

If we furthermore assume that for Silicon the perpendicular' interaction has an interaction length of 1 um, or 3300 atoms, deep, the height we need to get an interaction of 10^7 atoms would be easily calculated; $10^7 = x^2 * 3300 \implies x = \sqrt{\frac{10^7}{3300}} = 55$ atoms. Or an island of about 20x20 nm while being 1000nm high. Such a pillar would be extremely unstable and impossible to create with the beam-size of our current Focused Ion Beam (FIB) setup.

In the measurements for different depths we do observe a small increase in friction for the higher islands. Clearly, this is counter to what we would expect based on the idea that a higher island would consist of fewer atoms and subsequently fewer phonons to disperse the energy. I expect this to be the result of one, or a combination of two, effects. The first effect focuses on the method of the created islands. The islands are created by milling trenches using FIB (section 3.3). The FIB uses a Gaussian beam profile. Although the beam is focused it will still have tails of the Gaussian, which shine next to the created trenches. The deeper we mill, the longer our exposure time is and the more

we expect the tails of the beam to interact with the created island. This might result in a rounded shape of the island or otherwise changing the surface. The second effect is that the higher islands could be more susceptible to wear. As they have no atoms around them, it might be easier for atoms to break of the islands into the surrounding trenches. Furthermore, like the SEM described in appendix A, the FIB is not in Ultra High Vacuum. It is likely that we have some Carbon deposition during the milling. This might further change the top layer of our sample.

To try and reproduce the two-dimensional behaviour of MoS_2 we used 'oriented' MOST (section 4.3). For the islands on MOST we did see a factor 30(3) change in the friction. This change clearly correlates with the effective stiffness of the contact. More specifically, we see a clear linear correlation between friction and stiffness. This is very interesting, especially since this is not generally reported in literature. It is also not what we see for other materials (for example figure 4.4), where we see that the stiffness stays constant, even as the friction changes. Interestingly this factor 30(3) change in friction for the MOST sample (section 4.3) behaves comparable to the effect measured by Wada et al. [9], implying that perhaps they too were measuring an effect unrelated to the sizes of the islands.

Chapter 6

Conclusion and future work

The central question that led to this research was threefold. To investigate the details of lateral force microscopy as method to probe friction at the single asperity scale. To elaborate on a novel theory of how nanoscale adhesive friction functions through delocalized phonons. And finally, to propose and attempt experiments to test this theory.

For Lateral Force Microscopy (LFM) we have developed a method to measure friction and coefficients of friction on the nanoscale, through calibration of normal and lateral forces. We have implemented a method to measure the AFM tips within the AFM through deconvolution, which allowes us to not only investigate friction but also single asperity wear behaviour. Finally, we have investigated a Fourier based method to test whether periodic behaviour in our data is intrinsic or external of nature. As a result we are now able to investigate the origin of nanoscopic friction as well as investigate the more industrial challenges that ASML faces.

As a solution to the origin of nanoscale adhesive friction, we propose a novel theory from Frenken and Krylov. This theory explains the experimentally instantaneous energy damping through the dephasing of phonons. The important part is that friction is the effect of a localized interaction described through delocalized phonons. This delocalized interaction would depend on how many atoms are in the system, allowing us to test the theory experimentally through nano-patterned structures.

Our experimental tests on the created islands did not show a dependency of the friction on island size. Neither for Silicon wafer nor the worn MOST coating. For the measurements on MOST we did observe a factor 30(3) change in friction. We also observe a clear correlation between this change in friction and the interaction stiffness. To test if a dependency of friction on interacting atoms can be measured in even smaller systems,

we propose to use either a truly layered material with weak perpendicular interaction or ultra-thin samples.

Promising measurements that might lead to future endeavours are discussed in appendices B and D. In appendix B we have shown a sliding speed dependency for nanoscale friction. This is similar to results from Jacobs et al. who have reported a dependency on sliding speed for nanoscale wear [38]. The shown humidity dependency can be investigated more rigorously with the new gas flow cell. Furthermore, comparing our results with TRIS [42], a model which includes capillary forces in single asperity contacts, might lead to a deeper understanding of the effects of humidity. Appendix D shows that we now have everything we need to investigate Vapor Phase Lubrication (VPL) in nanoscale experiments. This might provide input to better understand the effects we have observed in macroscale experiments.

Finally, this project has been a first step for the *Contact Dynamics* group into the fundamentals of single-asperity contacts, a research direction that both the group and relevant research groups at ASML will continue for a deeper understanding into the fundamentals of friction.

Appendix A

Tip characterization by SEM

To quantitatively analyze the wear of AFM tips, we visualized tips through Scanning Electron Microscopy (SEM). These measurements were done using the Verios-SEM available at the AMOLF Nanolab. The SEM images can also be used to accurately measure the dimension of the cantilever, to accurately calculate the rotational stiffness as explained in section 2.5. In this appendix we will discuss how the SEM works, the measurements we did and what problems we encountered, which led us to instead use deconvolution as described in section 2.7.

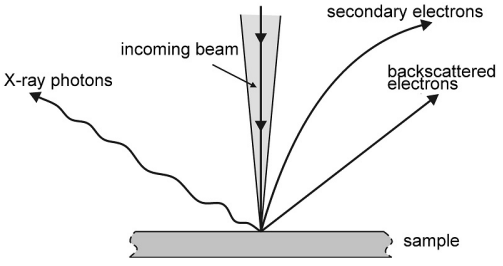

(A) Schematics of the produced electrons and photons in the SEM

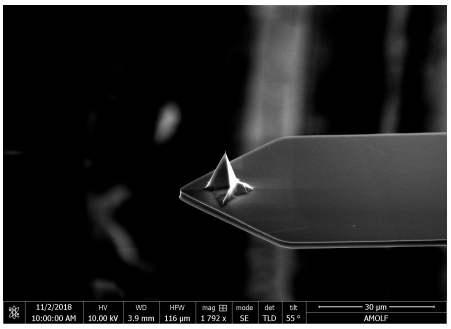

(B) SEM image of the AFM cantilever used to do our nano-scale friction measurements

The SEM exposes the sample surface to a focused beam of electrons. The electrons interact with atoms in the sample, producing electrons and photons as shown in figure A.1a. The intensity of the electrons maps the topography of the surface. The X-ray photons can be used to characterize the elements in the surface. The photons are produced because the incoming high energy electrons are equally likely to interact with outer shell electrons as with inner shell electrons. Interaction with inner shell electrons will create low energy holes. As an outer shell electron falls back to this lower energy, it emits the difference in energy as a photon. As these transition energies are element specific, the resulting spectrum reveals the composition of our sample. This is called

Energy-Dispersive X-ray Spectroscopy (EDS/EDXS)[1]. The probing depth is in the order of 0.1-10 μm depending on the incident energy [10].

Figure A.2 shows two images of the same AFM tip taken subsequently. Clear substantial deposition takes place in the SEM, even after only a few minutes of exposure. Furthermore, these images were taken at maximum resolution but are not clear enough to resolve the tip radius.

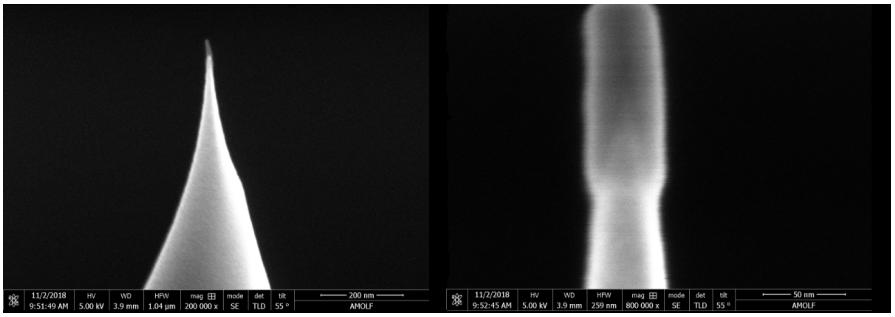

FIGURE A.2: Before (left) and after (right) images by SEM of an AFM tip.

To investigate which material deposits onto the tip we performed EDS creating the spectrum shown in figure A.3a. Figure A.3b shows where the four major elements are located. We can clearly see that the growth consists of Carbon and Oxide, while the tip consists of Silicon. We also see a higher brightness for Silicon in the growth but this is an artifact because of the increase of photon scattering compared to air, and comparable behavior of Silicon to Carbon. It is not bright enough to expect Silicon in the growth. The Aluminum we see in the background is the sample holder, which holds the tip in the SEM.

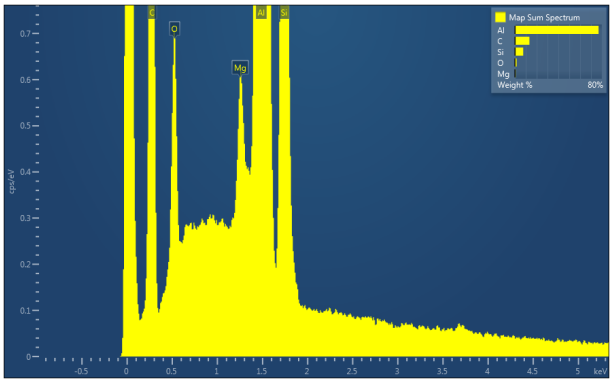

(A) EDS spectra, where the peaks are labeled with their likely sources

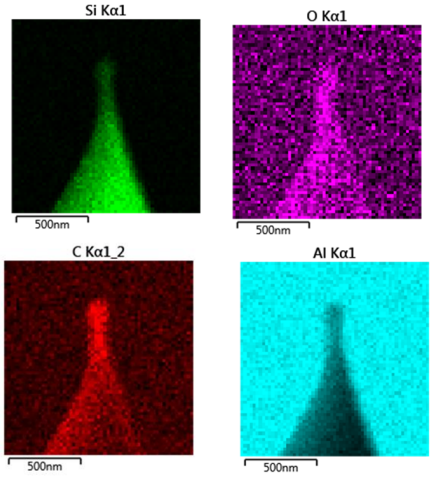

(B) EDS maps of the 4 dominant elements; Silicon, Oxygen, Carbon and Aluminum

[1] A good source of extra information can be found at: `www.jeol.co.jp/en/applications/pdf/sm/sem_atoz_all.pdf`

Appendix B

Other LFM dependencies

In this appendix we will present some other dependencies of the environment friction on environmental or machine parameters. In most cases it was unclear to us why these dependencies were as they were. And in all cases they are not needed for the central questions in this thesis.

B.1 Pull off dependence on the Humidity

Using the ramping measurements as explained in section 2.3 we have investigated the dependence of the adhesion force on Relative Humidity (RH). This was done to correspond to work by another student (Sander de Graaf) who has investigated the effect of humidity on macroscopic friction. The results presented in this section have been done through a quite crude setup in which we filled the AFM enclosure with dry Nitrogen gas (N_2) and measured the humidity by a hand held hygrometer [1]. It is possible to do more precise measurements through the new *gas flow cell* as used in appendix D.

Figure B.1 shows the adhesive/pull-off force as a function of the Relative Humidity (RH), we clearly see that an increased humidity increases the pull-off force with about 20%, this is in accordance with theory [43]. We expect this difference in pull-off force to be because of the formation of capillary bridges between the tip and the sample [44] If can be interesting to expand this research to high humidity's with the new flow cell to compare with the large base of existing literature [45].

[1] official name of a device that measure the humidity in air

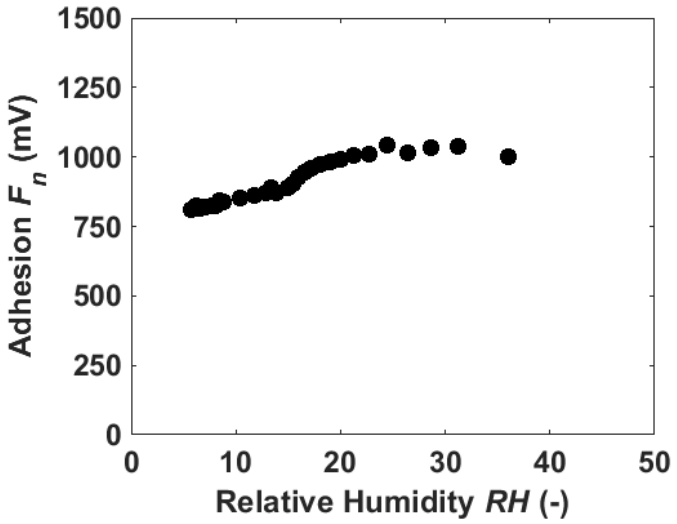

FIGURE B.1: Dependence of Adhesion Force on the Relative Humidity (RH). Ramps where done with 0.08(2) V relative Trigger Threshold (which corresponds to 3.1(9) nN), at 100 nm/s speed.

B.2 Speed Dependence

For macroscopic friction we know that varying the speed between two dry interacting surfaces does not change the friction. For nanoscopic interaction is is not necessarily so straight forward as Jacobs et al. [38] have already shown a speed dependence on speed for the wearing of the tip. Figure B.2a shows that we too observe a slight change in friction as we change the sliding speed. We do not clearly understand the details of this change. For the central question of this thesis we decided use a constant speed when comparing measurements and not focus on this observed change, but it does allow further investigation.

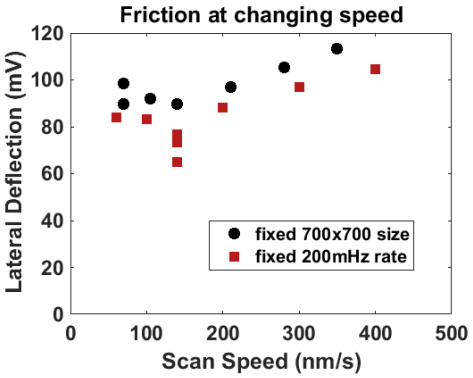

(A) Speed dependence of the friction. First the rate was increased subsequently the size was increased.

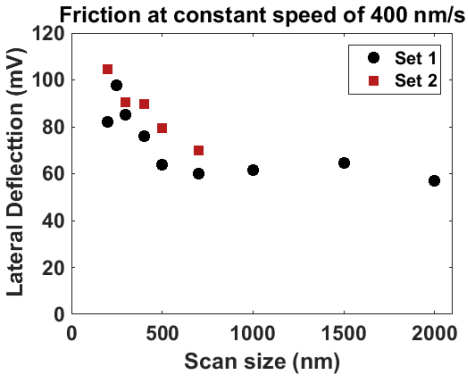

(B) Dependence of Friction on the Scan Size at constant speed. Set 1 and 2 where done subsequently with increasing size.

FIGURE B.2: Scans where done with VESPA-V2 tip at 1.75(5) V normal force (66(4) nN) and 128x128 lines on a Silicon wafer.

Appendix C

Peak Force Tapping mode (Scan Assist)

Peakforce QNM or Peakforce Tapping mode is a Bruker exclusive scanning mode which is based on the ramping procedure explained in section 2.3. It is an extended version of ScanAsyst® mode which is broadly used for topography measurements. Apart from the advantages discussed in this appendix, it is also the preferred method to measure the Roughness Sample as discussed in section 2.7.

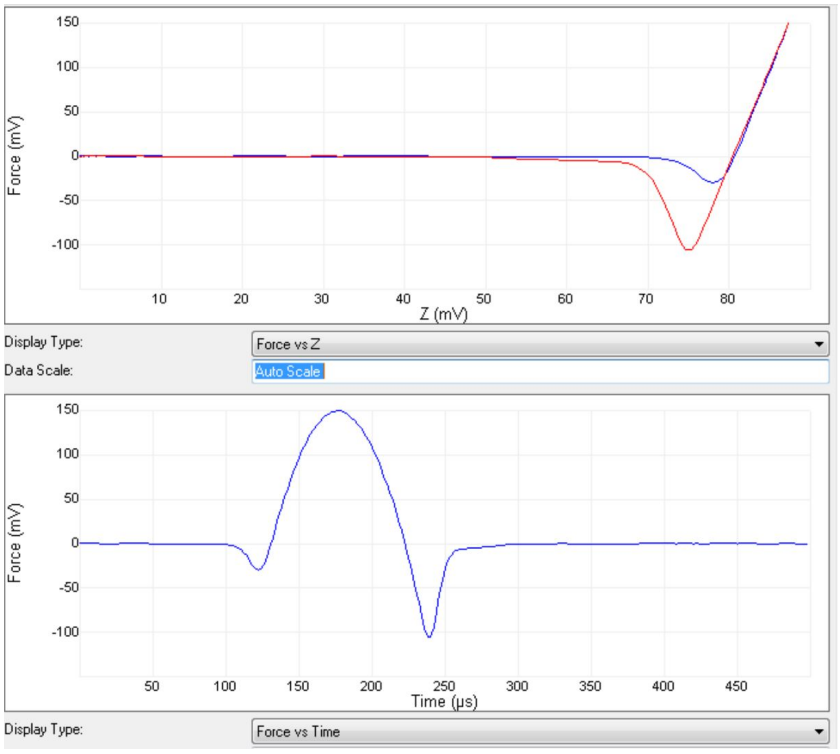

FIGURE C.1: Example of the Peakforce curve of a Sapphire sphere measured with an RTESPA tip. The upper curve is also shown in Scan Asyst.

In figure C.1 we see an example of a single Peakforce curve. The curve shows a single ramp, many of which are done to probe the surface. If we look at the bottom picture we see that the x-axis goes from 0 to 500 μs showing that the tip is ramping the surface at 2000 Hz, within the newest version of Nanoscope it possible to vary this rate. Equivalent to standard ramping, the tip starts free-hanging in the air (force is 0), approaches the surface till the 'snap-in' (around 100μs in the example). After 'snap-in', the tip pushes down further until it reaches the *peakforce*, after which the tip starts to retract. As with ramping, the tip sticks to the surface because of the adhesive force. Only when the puling force can overcome the adhesive force, the tip will 'snap-off' (around 24μs in figure C.1).

The advantage of Peakforce lies in the extra information it can calculate using the snap-in, adhesion and height profile. Because the ramping procedure gives much more direct information to the AFM software than for example tapping-mode or contact-mode, the software is able to self optimize changing the Peak Force setpoint (the extra force applied in the ramp) and the *integral gain* to get optimal overlap between trace and retrace while limiting damage to either tip or sample. This automation of the optimization procedure is also what makes ScanAsyst suited for infrequent users. Because one can get optimized profiles without minimal knowledge of machine or system. A second result is that this location specific information on the adhesion can be compared to the height profile to investigate whether the sample are all the same material. An example of this can be seen in figure C.2 where we see that the growth on the wear scar have much higher adhesive force implying that they are a softer material.

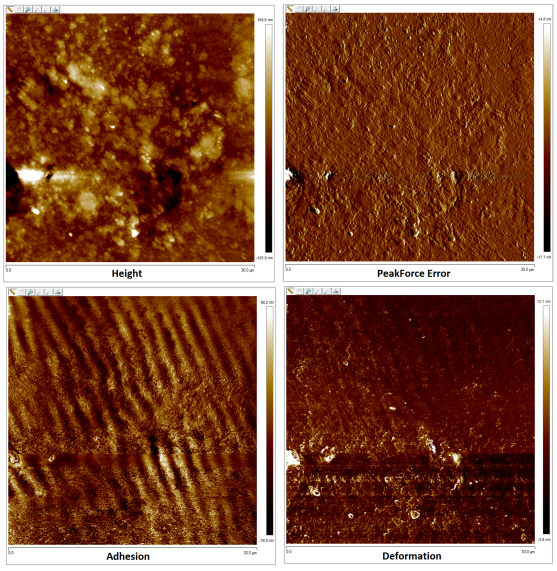

FIGURE C.2: Examples of different local data than can be obtained through PeakForce QNM

A final application of this method is to differentiate between hydrophobic and hydrophilic materials. These are expected to be covered in water films of varying thickness, potentially resulting in different capillary adhesion forces. The *EUV Photoresists group* at ARCNL is investigating a photoresist that changes hydrophobicity under EUV but does not change thickness. Together with a PHD-student (Olivier Lugier) of the *EUV Photoresist group*, I tried to measure a change in adhesion force for the exposed parts. Sadly we could not measure a difference larger than the general noise. The new version of Nanoscope does allow for PeakForce speeds down to 250 Hz. Perhaps this slower measurement in combination with noise reduction because of the new pump could work, but I expect that the effect would still be too small to be effective as probing mechanism.

Appendix D

Friction and wear with VPL

As final part of this project I looked whether we could reproduce the decrease in friction and wear observed by another Master student (*Daan Haver*) in macrosystems by using Isopropanol for Vapor Phase as Lubrication (VPL). This work was done together with a PHD-student (*Feng-Chun Hsia*) from the *Contact Dynamics group*. All details on the VPL effect can be found in the master thesis of *Daan Haver* named *'Tunable friction through isopropanol vapor phase lubrication: How does it work?'*.

This is placed in the appendix as it is not relevant to the central question of this thesis but is included as an example nanoscale experiment to investigate observed macroscale behaviour. And because it uses many of the investigated techniques from chapter 2 in an experimental application. It is relevant to the ASML application, if we suppress the wear of the asperities our contact would stay exactly the same which would allow us to better position the wafers on the wafer table.

D.1 Setup

The experiments were done in the same Bruker AFM. With the addition of an add-on gasflow cell. A picture of the setup is shown in figure D.1. An important observation is that we do not use the supplied fluid cantilever from Bruker but instead use the standard cantilever. This was done so we could apply the lateral calibration as explained in section 2.5.

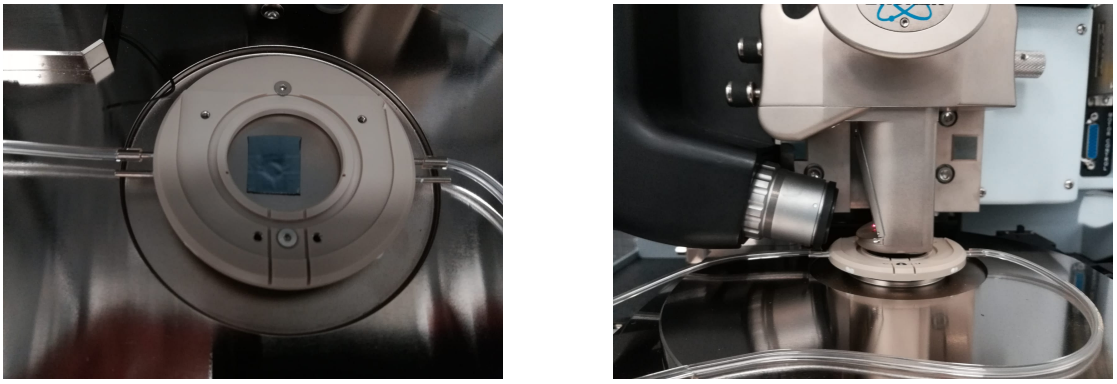

(A) Picture of our gas-flow-cell (B) Picture of the scanner in the flowcell

FIGURE D.1: Flowcell

The experiments are all done in; Ambient condition (RH 60%), Nitrogen flow and Isopropanol saturated Nitrogen flow. The motivation to also test with Nitrogen is to control whether the measured effect is because of Isopropanol or because of the carrier gas. A secondary comparison is that it represents a very dry environment (RH $< 5\%$), compared to the *Ambient* case.

D.2 Adhesion

Feng-Chun did Adhesion measurements comparing Ambient to VPL (figure D.2). These measurements where done by the ramping procedure (section 2.3). The chamber/sample was filled with VPL for at least 2 minutes. After using VPL a clean sample was used and the chamber got the chance to outgas for at least 10 minutes. We investigated the effect of VPL for Silicon, glass and PMMA to look at how VPL interacts differently. Glass and PMMA were chosen because these were already used in macro-scale rheometer experiments by *Daan Haver*.

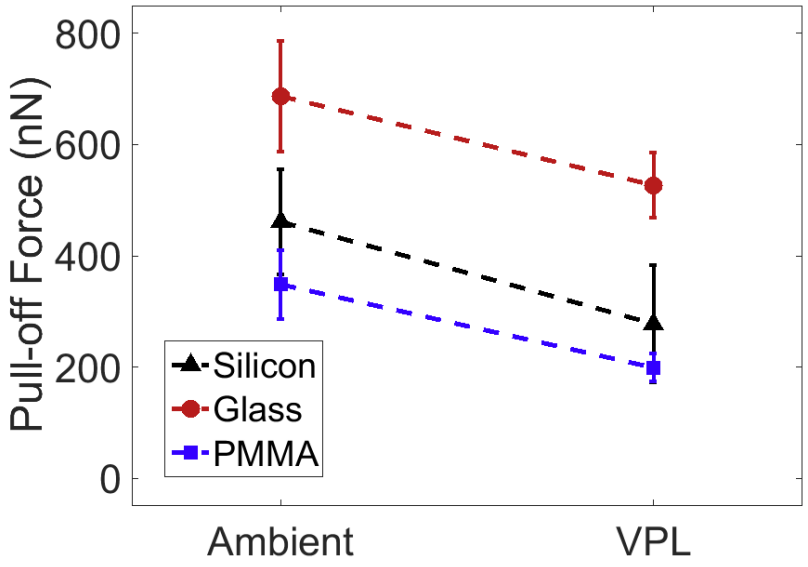

FIGURE D.2: Adhesion measurements, between Ambient and VPL. Speed of the ramp was 100nm/s with a trigger threshold of 200mV which represents a normal force of $2.6(4)\mu N$

We see a clear decrease in the adhesion force when switching from Ambient to VPL. This effect is observed for all three investigated materials. It might be part of the reason why we observe a decrease in Friction when introducing VPL as presented in the following section. The adhesion result results for the nitrogen environment are not presented because of experimental difficulties.

D.3 Friction

All of the measurements were done subsequently with the same tip. First we measured ambient. Next blew dry nitrogen gas into the cell for 5 minutes and kept the flow going while measuring. Finally, we repeated this procedure using Isopropanol Vapor. We waited for at least 20 minutes to let the tip diffuse all the VPL, and replaced the sample with a clean silicon wafer. We repeated this experiment three times with the same tip and presented the average friction. Figure D.3b shows the friction for three different normal forces in all three environments. The shown data points are averages of three measurements each.

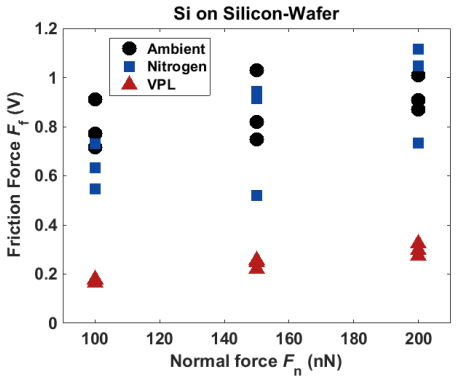

(A) Friction forces in Volts.

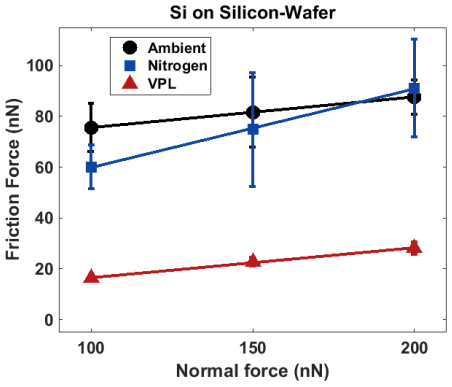

(B) The average Friction Force.

FIGURE D.3: The average Friction Force (F_f) versus normal Force (F_n), at $10\mu m/s$ with 30 lines of 5 μm each using a soft ESPA-V2 tip ($k \approx 0.2N/m$).

We clearly see that the friction decreases when flowing Vapor phase Isopropanol into the system. We also see that the error bars for the VPL case are much smaller indicating a more stable interaction. Both these observations can also be made in macroscale experiments. It is also interesting that all three environments have a comparable slope when increasing the normal force.

D.4 Wear

To measure the wear over time we did 9 scans each of 5.12 mm (512 lines x 2 x 5 μm per line), at 100nN normal force. Each environment was measured with one dedicated soft ESPA-V2 tip. We measure the tip radius through deconvolution before starting and after each set of 3 scans (figure D.4b). During wearing we also measure the friction, the averages of which are presented in Figure D.4a. Figure D.4c shows the normalized wear, where we see more clearly that the VPL really suppresses the wear of the tip.

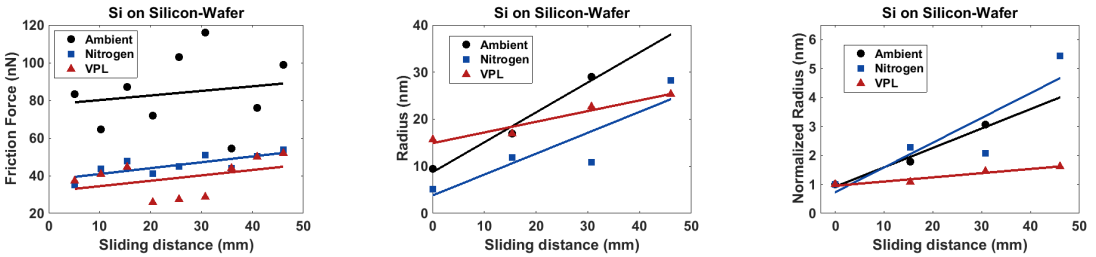

(A) Friction during wear (B) Tip radius (C) Normalized tip radius

FIGURE D.4: Friction and tipradius during VPL wear experiment

Regretfully our starting tip size for VPL was substantially larger then for Ambient or Nitrogen hampering our comparison. Nonetheless we see that although VPL started with the largest tip after 9 scans it had the smallest, clearly indicating a lower wear rate. This is extra pronounced in the normalized tip radius in figure D.4c, although this might be an overly positive representation. As follow up to our observed correlation between Friction and stiffness for MoST (section 4.3) we also compare friction and stiffness for these VPL experiments in figure D.5.

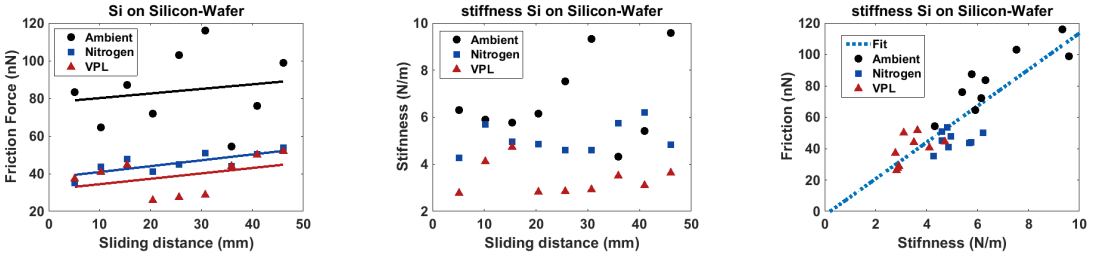

(A) Friction during wear (B) Stiffness (C) Friction vs Stiffness, with linear fit

FIGURE D.5: Comparing friction and stiffness within the VPL wear experiment

Figure D.5c shows a correlation between the friction and the effective stiffness at the tip-surface interface. The linear fit has a slope of 11(3) and offset of -2(8), which I assume should be zero in the ideal case. The fit has an R square of 0.75, which is reasonable but not a definitive result. But this first measurement does imply a possible mechanism though which the Isopropanol vapour decreases the friction.

Appendix E

Utrecht SPM day 2018

As part of the LFM measurements development, I went to the *Utrecht Dutch Scanning Probe Microscopy Day 2018*[1] to present our provisional results and see which other groups in the Netherlands work with similar methods. To show our first steps and elicit interest I also presented a poster, which you can find on the next page. In this appendix, we will briefly explain the presented results and how these have motivated the work in this thesis.

Under the header; '*Worn MoST coated SiC*', we presented the experimental setup. A macro-scale friction measurement was done with a 3 mm Silicon Carbide (SiC) sphere coated with a Molybdenum di-Sulfide Titanium composite (MoST)[37]. The coating was 500nm thick and between the SiC and MoST coating was a 100nm thick Titanium layer to aid adhesion. The coated sphere was rubbed over a flat silicon wafer for *6m*, using the UMT, at *0.1N* normal force. As we see in the optical image the coating is worn through revealing 3 different areas. We compared the measured friction in the unworn MoST, the worn ring of MoST and the center which we expect to be the Titanium adhesion layer.

Under the header; '*Lateral Force Microscopy (LFM)*', we showed plots comparing the average friction for three independent sets of measurements. The plots clearly show a discrepancy in absolute numbers but they show a similarity in behavior when comparing different regions. This becomes clear when we plot the ratio between different sets as shown under *Conclusions*. The problem in obtaining absolute values led us to delve into ways to correctly calibrate the lateral force, the results of which are presented in section 2.5. The observed change because of tip-wear is further investigated in section 2.7.

[1] http://www.swartlab.eu/spm_day.html

Bibliography

[1] Richard P Feynman. Plenty of room at the bottom. In *APS annual meeting*, 1959.

[2] Gerd Binnig, Calvin F Quate, and Ch Gerber. Atomic force microscope. *Physical review letters*, 56:930, 1986.

[3] Kenneth Holmberg and Ali Erdemir. Influence of tribology on global energy consumption, costs and emissions. *Friction*, 5:263–284, 2017.

[4] Abdoulaye Fall, B Weber, M Pakpour, Nicolas Lenoir, N Shahidzadeh, J Fiscina, C Wagner, and Daniel Bonn. Sliding friction on wet and dry sand. *Physical review letters*, 112:175502, 2014.

[5] Ian M Hutchings. Leonardo da vinci's studies of friction. *Wear*, 360:51–66, 2016.

[6] Guillaume Amontons. De la résistance causée dans les machines. *Imprimerie royale (Paris)*, 1699.

[7] AI Vakis, VA Yastrebov, J Scheibert, L Nicola, D Dini, C Minfray, A Almqvist, M Paggi, Seunghwan Lee, G Limbert, et al. Modeling and simulation in tribology across scales: An overview. *Tribology International*, 125:169–199, 2018.

[8] Ma Renfeng, Joost Frenken, and Sergey Krylov. Hit the brakes; friction without dissipation. *[under review]*, 2019.

[9] Noriyuki Wada, Makoto Ishikawa, Takuma Shiga, Junichiro Shiomi, Masaru Suzuki, and Kouji Miura. Superlubrication by phonon confinement. *Physical Review B*, 97:161403, 4 2018.

[10] Kenjiro Oura, VG Lifshits, AA Saranin, AV Zotov, and M Katayama. *Surface science: an introduction*. Springer Science & Business Media, 2013.

[11] Arzu Çolak, Herbert Wormeester, Harold J.W. Zandvliet, and Bene Poelsema. The influence of instrumental parameters on the adhesion force in a flat-on-rough contact geometry. *Applied Surface Science*, 353:1285–1290, 2015.

[12] Arzu Colak, Herbert Wormeester, Harold JW Zandvliet, and Bene Poelsema. Surface adhesion and its dependence on surface roughness and humidity measured with a flat tip. *Applied surface science*, 258:6938–6942, 2012.

[13] Bhushan Bharat. *Springer Handbook of Nanotechnology*. Springer, 2004.

[14] Tomislav Suhina, Bart Weber, Chantal E Carpentier, Kinga Lorincz, Peter Schall, Daniel Bonn, and Albert M Brouwer. Fluorescence microscopy visualization of contacts between objects. *Angewandte Chemie*, 127:3759–3762, 2015.

[15] Jeffrey L Hutter and John Bechhoefer. Calibration of atomic-force microscope tips. *Review of Scientific Instruments*, 64:1868–1873, 1993.

[16] Manuel LB Palacio and Bharat Bhushan. Normal and lateral force calibration techniques for AFM cantilevers. *Critical Reviews in Solid State and Materials Sciences*, 35:73–104, 2010.

[17] Feng-Chun Hsia, Dai-Ming Tang, Wipakorn Jevasuwan, Naoki Fukata, Xin Zhou, Masanori Mitome, Yoshio Bando, Torbjörn EM Nordling, and Dmitri Golberg. Realization and direct observation of five normal and parametric modes in silicon nanowire resonators by in situ transmission electron microscopy. *Nanoscale Advances*, 2019.

[18] Dror Sarid. *Scanning force microscopy: with applications to electric, magnetic, and atomic forces*, volume 5. Oxford University Press on Demand, 1994.

[19] F. Hausen and P. Egberts. Atomic-Scale Friction. *Encyclopedia of Interfacial Chemistry*, pages 40–54, 2018.

[20] M Varenberg, I Etsion, and G Halperin. An improved wedge calibration method for lateral force in atomic force microscopy. *Review of scientific instruments*, 74: 3362–3367, 2003.

[21] Manuel LB Palacio and Bharat Bhushan. Normal and lateral force calibration techniques for afm cantilevers. *Critical Reviews in Solid State and Materials Sciences*, 35:73–104, 2010.

[22] CT Gibson, Gregory S Watson, and S Myhra. Scanning force microscopy, calibrative procedures for 'best practice'. *Scanning*, 19:564–581, 1997.

[23] Koo-Hyun Chung. Wear characteristics of atomic force microscopy tips: A review. *International journal of precision engineering and manufacturing*, 15:2219–2230, 2014.

[24] Tevis D.B. Jacobs, Graham E. Wabiszewski, Alexander J. Goodman, and Robert W. Carpick. Characterizing nanoscale scanning probes using electron microscopy: A novel fixture and a practical guide. *Review of Scientific Instruments*, 87, 2016.

[25] Tevis D B Jacobs and Robert W Carpick. Nanoscale wear as a stress-assisted chemical reaction. *Nature Nanotechnology*, 8:108–112, 2013.

[26] Erin E Flater, Jared D Barnes, Jesse A Hitz Graff, Jayse M Weaver, Naveed Ansari, Aimee R Poda, W Robert Ashurst, Subarna R Khanal, and Tevis DB Jacobs. A simple atomic force microscope-based method for quantifying wear of sliding probes. *Review of Scientific Instruments*, 89:113708, 2018.

[27] Daan Vorselen, Ernst S Kooreman, Gijs JL Wuite, and Wouter H Roos. Controlled tip wear on high roughness surfaces yields gradual broadening and rounding of cantilever tips. *Scientific reports*, 6:36972, 2016.

[28] Matteo Frigo and Steven G Johnson. Fftw: An adaptive software architecture for the fft. volume 3, pages 1381–1384, 1998.

[29] Ernst Meyer and Enrico Gnecco. Superlubricity on the nanometer scale. *Friction*, 2:106–113, 2014.

[30] GA Tomlinson. Cvi. a molecular theory of friction. *The London, Edinburgh, and Dublin philosophical magazine and journal of science*, 7:905–939, 1929.

[31] Ludwig Prandtl. Ein gedankenmodell zur kinetischen theorie der festen körper. *ZAMM-Journal of Applied Mathematics and Mechanics/Zeitschrift für Angewandte Mathematik und Mechanik*, 8:85–106, 1928.

[32] Dirk W van Baarle, Sergey Yu Krylov, ME Stefan Beck, and Joost WM Frenken. On the non-trivial origin of atomic-scale patterns in friction force microscopy. *Tribology Letters*, 67:15, 2019.

[33] A Buldum, DM Leitner, and S Ciraci. Model for phononic energy dissipation in friction. *Physical Review B*, 59:16042, 1999.

[34] Lucille A Giannuzzi and Frederick A Stevie. A review of focused ion beam milling techniques for tem specimen preparation. *Micron*, 30:197–204, 1999.

[35] Robert W Carpick, DF Ogletree, and Miguel Salmeron. Lateral stiffness: A new nanomechanical measurement for the determination of shear strengths with friction force microscopy. *Applied Physics Letters*, 70:1548–1550, 1997.

[36] Yalin Dong, Qunyang Li, and Ashlie Martini. Molecular dynamics simulation of atomic friction: A review and guide. *Journal of Vacuum Science & Technology A: Vacuum, Surfaces, and Films*, 31:030801, 2013.

[37] Xin Wang, Yanmei Xing, Shengli Ma, Xiaoling Zhang, Kewei Xu, and D. G. Teer. Microstructure and mechanical properties of MoS2/titanium composite coatings with different titanium content. *Surface and Coatings Technology*, 201:5290–5293, 2007.

[38] Yuchong Shao, Tevis DB Jacobs, Yijie Jiang, Kevin T Turner, Robert W Carpick, and Michael L Falk. Multibond model of single-asperity tribochemical wear at the nanoscale. *ACS applied materials & interfaces*, 9:35333–35340, 2017.

[39] Lars Pastewka and Mark O Robbins. Contact between rough surfaces and a criterion for macroscopic adhesion. *Proceedings of the National Academy of Sciences*, 111:3298–3303, 2014.

[40] Arzu Çolak, Herbert Wormeester, Harold JW Zandvliet, and Bene Poelsema. The influence of instrumental parameters on the adhesion force in a flat-on-rough contact geometry. *Applied surface science*, 353:1285–1290, 2015.

[41] Yasuhisa Ando. Effect of contact geometry on the pull-off force evaluated under high-vacuum and humid atmospheric conditions. *Langmuir*, 24:1418–1424, 2008.

[42] M Bazrafshan, MB de Rooij, and DJ Schipper. Adhesive force model at a rough interface in the presence of thin water films: The role of relative humidity. *International journal of mechanical sciences*, 140:471–485, 2018.

[43] Robert Jones, Hubert M Pollock, Jamie AS Cleaver, and Christopher S Hodges. Adhesion forces between glass and silicon surfaces in air studied by afm: Effects of relative humidity, particle size, roughness, and surface treatment. *Langmuir*, 18: 8045–8055, 2002.

[44] Shengfeng Cheng and Mark O Robbins. Capillary adhesion at the nanometer scale. *Physical Review E*, 89:062402, 2014.

[45] Aaron J. Harrison, David S. Corti, and Stephen P. Beaudoin. Capillary Forces in Nanoparticle Adhesion: A Review of AFM Methods. *Particulate Science and Technology*, 33:526–538, 2015.